ISSN 1831-9424

European Commission

JRC TECHNICAL REPORT

CO_2 measurements in ambient air: testing of SenseAir K96 low-cost sensor

Yatkin, S., Gerboles, M., Manca, G. and Signorini, M.

2023

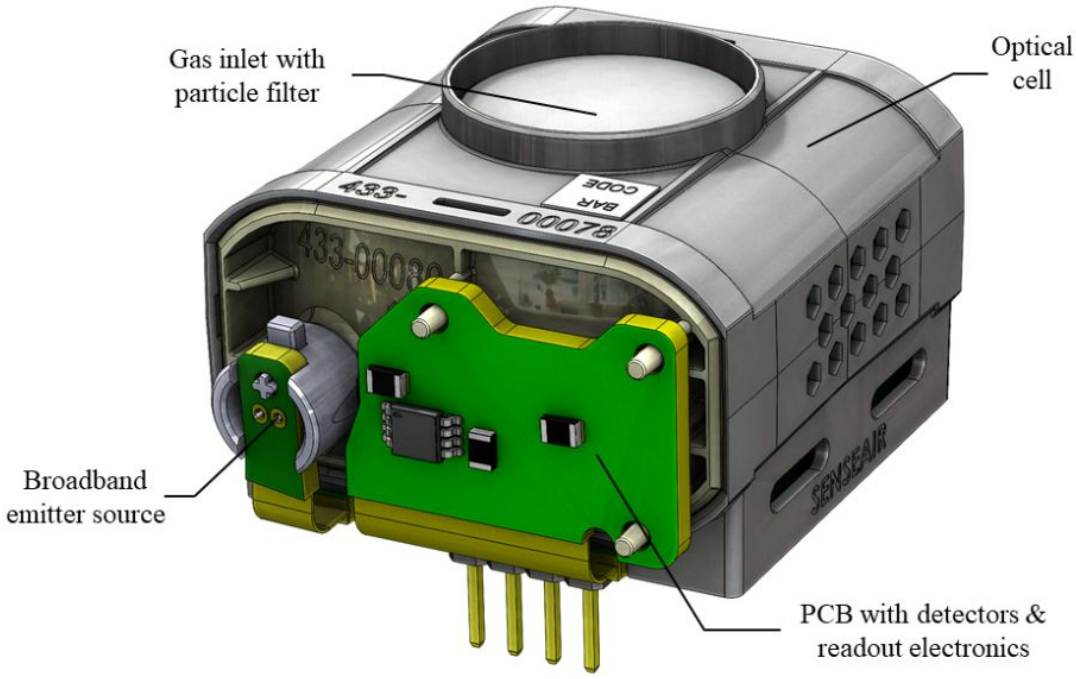

Joint Research Centre

EUR 31403 EN

Contact information
Name: Sinan Yatkin
Address:
Email: sinan.yatkin@ec.europa.eu
Tel.: +39 0332 786201

EU Science Hub
https://joint-research-centre.ec.europa.eu

JRC132309

EUR 31403 EN

PDF ISBN 978-92-76-62089-1 ISSN 1831-9424 doi:10.2760/31673 KJ-NA-31-403-EN-N

Luxembourg: Publications Office of the European Union, 2023

How to cite this report: Yatkin, S., Gerboles, M., Manca, G. and Signorini, M, *CO2 measurements in ambient air: testing of SenseAir K96 low-cost sensor*, Publications Office of the European Union, Luxembourg, 2023, doi:10.2760/31673, JRC132309.

Contents

Abstract

An AirSensEUR sensor system equipped with a prototype CO_2 low-cost sensor (LCS), model K96 Senseair, has been tested at the Joint Research Centre (JRC) observatory station between December 2021 and September 2022 in order to evaluate whether its expanded measurement uncertainty could meet a Data Quality Objective (DQO) of 10 ppm.

Firstly, the K96 LCS has been integrated into the JRC AirSensEUR sensor system, for which a measuring chamber with temperature control capacity set at 25 °C was designed. Additionally, a reference Picarro G2401 has been placed on the roof of the JRC observatory station at less than 50 cm away from the AirSensEUR sensor system. The Picarro measurements were used as reference CO_2 data for comparing with K96 sensor data and for sensor calibration once the Picarro was adjusted for calibration drift.

We calibrated the wet K96 LCS data against wet CO_2 Picarro reference data. Linear models were found unreliable as residuals of the model were strongly associated with water vapour and temperature in the measuring chamber, and with air pressure to a lower extent. A multiple linear model was finally used for calibration using water vapour and air pressure in the measuring chamber as covariates.

Applying this calibration, the expanded uncertainty of hourly LCS measurements remained below the DQO between February and early June 2022 when the reference CO_2 was between 380 and 550 ppm as well as the temperature in the measuring was maintained around 25 °C. This result is promising, as the measurement uncertainty of K96 LCS was found three times smaller than the lowest measurement uncertainty claimed by the other manufacturers of CO_2 LCSs available in the market.

However, from June 2022, the newly designed AirSensEUR measuring chamber was unable to maintain the set temperature of 25 °C due to the high air temperature recorded in summer 2022. As expected, the increased temperature triggered a drift of the K96 LCS measurements resulting in the measurement uncertainty of 25 ppm being higher than the DQO.

In the future, the software-operated control of temperature in the measuring chamber of AirSensEUR as well as better sun shielding shall be further developed and implemented to take the full benefit of the promising CO_2 measurement capacity of the K96 sensor when the set temperature is more precisely maintained.

Authors

Sinan Yatkin, Michel Gerboles, Giovanni Manca and Marco Signorini

1 Introduction

Uncertainties of fossil fuel carbon dioxide (CO_2) emissions from inventories based on statistics are in the order of 5 % for the Organisation for Economic Co-operation and Development (OECD) countries and up to 20 % in other countries. However, they are larger in the city-scale. Moreover, in many cities emission inventories are not available. The need for more reliable information on emissions and their trends in cities has prompted the development of a network of urban in-situ CO_2 observations based on commercially available low-cost sensors (LCSs). However, performance of these sensors must be evaluated against reference analysers prior to deployment in situ.

To support this evaluation, the ongoing testing activity of urban air quality low cost sensors carried out by the Joint Research Centre (JRC) in the framework of the European Parliament Pilot Project named "Integrating smart sensors and modelling for air quality monitoring in cities"([1]) is further expanded with field experiments at the Integrated Carbon Observation System (ICOS) class-2 atmospheric station at the JRC Atmospheric Observatory (Ispra, Italy) where CO_2 reference instrumentation is deployed. The results of performance evaluation tests of commercially available CO_2 LCS carried out at the JRC Atmospheric Observatory are presented in this report.

While for air quality monitoring using LCSs, data quality objectives (DQO) are already defined in the European Air Quality Directive ("2008/50/EC: Directive of the European Parliament and of the Council of 21 May 2008 on ambient air quality and cleaner air for Europe"), the DQO are not defined in legislation for CO_2 monitoring in urban areas.

Although, the ICOS programme has defined a DQO for CO_2 monitoring, expressed as the maximum deviation between daily checks of CO_2 reference measurements and the certified values of CO_2 mixtures in cylinders (0.1 ppm), such a stringent DQO is not convenient for LCSs measurements. In fact, one must consider that the objective of the ICOS programme is to make sure that any trend detected in CO_2 monitoring is caused by a change in CO_2 emissions, not by measurement artefact. Conversely, LCSs would be mainly used to detect significant differences between CO_2 measurements at two different locations within the same urban area. We want to be sure that these differences are caused by a local emission source rather than by LCSs measurement artefacts. The DQO for CO_2 LCS measurement can be set as 10 % of the smallest differences in two LCSs measurements that we want to detect with reasonable accuracy. If the smallest difference is set to 100 ppm, we end up with a DQO for CO_2 of 10 ppm of expanded measurement uncertainty.

The aforementioned DQO for CO_2 LCSs is more stringent than the one given in the European protocol for sensor performance evaluation ("CEN/TS 17660-1 Air quality — Performance evaluation of air quality sensor systems — Part 1: Gaseous pollutants in ambient air," 2021) which sets the DQO for CO_2 as 30 ppm

([1]) Pilot Project "Integrating smart sensors and modelling for air quality monitoring in cities" proposed by the European Parliament and implemented by the European Commission (Service contract no. 07027747/2019/812686/SER/ENV.C.3)

2 Carbon dioxide low cost sensors

2.1 Review of existing sensors

LCSs are only capable of sensing, and need additional electronic components in order to become fully operational air quality monitoring systems. LCSs are generally integrated into so- called "Sensor Systems", which also includes power supply and/or batteries, sampling capability, signal processing, local data storage, data transmission and protective box against extreme weather conditions. Those additional elements of Sensor Systems add up costs into sole cost of LCS. Other operational costs such as power supply, internet connection, data servers as well as personnel needed for selection of sampling sites, installation, calibration, maintenance, data validation and reporting also add up to total cost of air quality monitoring using LCSs.

Table 1 lists the most common LCSs used for monitoring CO_2 with manufacturer/brand model, the CO_2 measurement range in ppm, the accuracy claimed by manufacturers, size, price, comments, web links and some electrical aspects like current consumption, power supply, communication protocols etc. The most important parameter for selecting the best LCS is in the column "Claimed Accuracy for CO_2". None of the LCSs meet the DQO of 10 ppm.

Table 1. Short list of the most commonly commercially available low cost sensors for CO_2 monitoring

Company	Model	Range for CO_2 in ppm	Claimed accuracy for CO_2	Current Consumption	Power Supply	Interface and Communication protocols	Size, mm	Price Euro (2021)	Comments	Links
Senseair	S8	400-2000, (residential) 0-10000 (mini) Lifetime > 15 years	±70ppm ±3 %	Max Current: 300 mA peak, 30mA average	4.5 – 5.25 VDC,	UART, Modbus	33.9 x 19.8 x 8.7, 8 grams	99 $ at CO2meter.com on 2022-12-06	The S8 Miniature 10,000ppm (1%) Sensor module is designed to be used as a safety switch for indoor control and alarm applications like portable heaters or fresh air ventilation in cars. It is a leader in the next generation of small size, low power, NDIR ambient air CO_2 sensors. Low Power, Small Footprint Design, Automatic Background Calibration. **CM-0177 S8 CO2 Sensor Development Kit** - Easy to use, simply plug the sensor module into your PC via USB. Use our free GasLab® software to measure and graph carbon dioxide, to configure the sensor or for data logging.	https://rmtplusstoragesenseair.blob.core.windows.net/docs/publicerat/PSP107.pdf https://www.co2meter.com/products/s8-miniature-co2-sensor-1
Senseair	K30	0-10,000 Sensor Life Expectancy: > 15 years	Accuracy: 30 ppm ± 3 % (Yasuda et al., 2012) Repeatability: ± 20 ppm ± 1 % of measured value	Max: 300 mA Average: 70 mA	5-14 VDC	UART or I2C, + analog outputs	51 × 57 × 14	119 $ at CO2meter.com on 2022-12-06	The K30 FR Fast Response 10,000ppm CO_2 Sensor module is a maintenance-free CO_2 transmitter intended for higher sample rates (2x per second) with minimal noise. It is an accurate, low-cost solution for OEMs who want to integrate CO_2 sensing into applications like modified atmosphere packaging (MAP), occupancy detection, or rapid data sampling for process monitoring. **CM-0126 K30 FR Sensor Development Kit** - Easy to use, simply plug the K30 FR sensor module into your PC via USB. Use our free GasLab® software to measure and graph carbon dioxide levels, to configure the sensor or for data logging.	https://www.co2meter.com/products/k-30-fs-10-000ppm-co2-sensor
Senseair	LP8	0-10,000 Sensor Life Expectancy: > 15 years	± 50ppm, ± 3%	Max: 0.6 mA.	2.9-5.5 VDC	UART	32.7 × 19.7 × 8 mm (LxWxH) < 8 grams.	139 $ at CO2meter.com on 2022-12-06	The LP8 miniature 10,000 ppm CO_2 sensor is designed from the ground up for long-term battery or solar-powered applications. It utilizes a flexible CO_2 measurement period to minimize power consumption. It can be powered by 3 alkaline 1.5V batteries, or a single 3.6V Li-SOCl2 battery. Response Time: 30 seconds.. Maintenance Interval: no maintenance required. Self-Diagnostics: complete function check on startup. This is the sensor used in CarboSense (http://carbosense.wikidot.com/) CM-0217 Development Kit - Easy to use, simply plug the sensor module into your PC via USB.	https://www.co2meter.com/products/lp8-miniature-co2-sensor?variant=838767706132
Senseair	SunRise	400-10000 (SE-11 1%) 400-5000 (006-0-007), Lifetime > 15 years	±30 ppm ± 3%	Peak < 125 mA, Sampling: 99mA, Average 45µA	3.05-5.5 VDC	UART, I2C	33.5x19.7x11.5, 5 grams	229 $ at CO2meter.com on 2022-12-06 for SE-11 1 %	The Senseair Sunrise SE-11 1% CO_2 Sensor is a miniature sensor module for battery-powered applications. It gives full control over the sensor's integration into a host system, flexibility in changing of the CO_2 measurement period, and power consumption. The NDIR CO_2 sensor uses an LED light source that saves power and makes it resistant to vibration while maintaining high precision. It has a life expectancy of more than 15 years. The self-correcting ABC algorithm automatically calibrates the sensor and assures it will still be accurate which is key in wireless applications. Wide supply voltage range enables a variety of battery options. Robust and resistant to vibrations and tough environment. Self Calibration. High precision NDIR sensor with LED Technology. Adjustable measurement period by host. Adjustable ABC period by host. Ultra-low power consumption. Pressure dependence: 1.6 % per kPa deviation from normal pressure CM-11 CO2 Sensor Development Kit - Easy to use, simply plug the sensor module into your PC via USB. Use our free GasLab® software to measure and graph carbon dioxide, to configure the sensor or for data logging. Includes a connector and switch configurations to connect to an Arduino, Raspberry Pi, or any other microcontroller via UART or I2C for rapid development and prototyping.	https://www.co2meter.com/collections/senseair/products/se-11?variant=19838776868982 https://rmtplusstoragesenseair.blob.core.windows.net/docs/Dev/publicerat/PSH11649.pdf https://www.akm.com/eu/en/products/co2-sensor/lineup-co2-sensor/
Senseair	K33 ELG	0-10000 Sensor Life Expectancy: > 15 years	± 30ppm ± 3% RMSE 176 ppm (Harmon et al., 2015)	Max: 250 mA, Average 40 mA	6-14 VDC	UART or I2C,	2.0 × 2.25 × 0.5 inches	299 $ at CO2meter.com on 2022-12-06	The K33 ELG (environmental logger) is designed to log up to 10,000ppm (1%) carbon dioxide, temperature, and % relative humidity in ambient air. Because of its ultra-low power requirements, it can "wake up", take a sample, store the data in memory, and go back to sleep. Using battery power only, the sensor can be placed in the field for days or even weeks at a time. **CM-0026 K33 ELG 1% CO2 Sensor Development Kit** - Easy to use, simply plug the sensor module into your PC via USB. Use it for evaluation, rapid application development or for experiments. The Devkit includes a K33 ELG sensor with pre-soldered connectors that provide power and connectivity. UART to USB Bridge cable, universal power supply and AA battery pack included. Uses our free GasLab® software to measure and graph carbon dioxide, to configure the sensor or for data logging.	https://www.co2meter.com/products/k33-environmental-logger-co2-sensor
Senseair	K96	LPL channel 400–3000	CO_2: resolution 0.1 ppm, no data on uncertainty	Average: between 50 and 120 mA	6 – 8.5 V	UART, Modbus	43 x 34 X 26 mm	Commercial price not defined yet.	Confidential users guide. The K96 is an advanced prototype still under development	https://www.mdpi.com/2073-4433/13/11/1789

		SPL channel 400–8500						Contact Senseair AB		
ELT	S-100H	0 - 2000	30 ppm ± 5 % (Yasuda et al., 2012)	Average :16mA, Max:400mA	12 VDC	Analog Voltage, UART, I2C	39 x32 x18.5, 10g	Out of production		https://cdn-3a4dd4ab.ozdisan.com/ETicaret_Dosya/453392_4677536.pdf
ELT	D-300LG	0-2000	±30 ppm ±3%	Normal: 12 mA, Peak: < 180 mA, Sleep < 0.3 mA	3.2V ~ 3.6V	TTL-UART, I2C, Option (Analog Voltage, PWM)	33 x 33 x 13.1	120 Euros in 2021 at TecnoSens SpA	D-300(LG)-3V series is the smallest Dual CO_2 sensor module in the world. Its Persistent Stability and Temperature Effect Resistance are welcomed as HVAC in warehouse, greenhouse, hospitals etc. D-300(LG)-3V is much favored by customers whose application needs 3.3 Voltage input and sleep mode support so on. D-300LG sensor accept relative humidity up to 99 %	http://www.eltsensor.co.kr/2016/products/oem_modules/D-300.html
Sensirion	SCD30	400-10000, lifetime-15 years	±30 ppm + 3 % Repeatability: ± 10 ppm	19mA @ 1 meas. per 2 s	3.3V –5.5V	UART (Modbus Point to Point; TTL Logic), PWM and I^2C	35x23x7 mm	46.03 (DigiKey)	Integrated temperature and humidity sensor, Dual-channel detection for superior stability. Repeatability (3400 ppm –10'000 ppm): ± 10 ppm. Temperature stability (T = 0 ... 50°C): ± 2.5 ppm / °C. Response time ($\tau_{63\%}$): 20s Accuracy: drift over lifetime (400 ppm –10'000 ppm), ASC field-calibration algorithm activated and SCD30 in environment allowing for ASC, or FRC field-calibration algorithm applied:± 50ppm	https://media.digikey.com/pdf/Data%20Sheets/Sensirion%20PDFs/CD_DS_SCD30_Datasheet_D1.pdf
GSS	CozIR®-LP2	0-2000	30 ppm ± 3 %, Noise: 6 ppm	Normal: 15 mA, Peak: < 40, Sleep < 0.01 mA	3.25 – 5.5 VDC, typical 3.3 VDC	UART or I2C control and data interface	31 x 19.5 x 6.8	149 $ at CO2meter.com on 2022-12-09	Built-in auto-zeroing	https://gvzcomp.it/products-technologies-separator/qss?format=raw&task=download&fid=1877
GSS	CozIR®-AH-1 (CozIR®-A)	0-2000	30 ppm ± 3 %,	Normal: 15 mA, Peak: < 40, Sleep < 0.01 mA	3.25 – 5.5 VDC, typical 3.3 VDC	UART, analogue voltage	40.4 x 40.4 x 11.65	117 $ at https://it.rs-online.com/ on 2022-12-09	Built-in auto-calibration	https://docs.rs-online.com/f74a/A700000007095278.pdf
Vaisala	GMM22C		30 ppm ± 2 % (Yasuda et al., 2012)					Unknown		
Vaisala	GMP343	0-1000, 0-2000, 0-3000, 0-4000,0-5000, 0-2 %	0-1000 ppm: ±(3 ppm + 1 % of reading) 0-2000 ppm: ±(5 ppm + 2 % of reading)	Without optics heating : < 1 W, With optics heating : < 3.5 W	11-36 VDC	RS-485, RS-232	188 x fi 45 360 g	Contact Vaisala, It used to be 3000 Euro in 2021		https://docs.vaisala.com/v/u/B210688EN-H/en-US
Vaisala	GMP252	0 - 10 000	0-3000: ±40 ppm, 3000-10 000: ±2 % of reading,		12 ... 30 VDC digital output,	RS-485, Modbus	130 x fi 25 58 g	Contact Vaisala Unknown price		https://docs.vaisala.com/v/u/B211567EN-F/en-US

Source: JRC, 2022.

2.2 Presentation of sensor Senseair K96

The Senseair K96 sensor (Senseair - Sweden) is an advanced prototype still under development, cost-effective non-dispersive infrared (NDIR) multi-gas sensor aimed at environmental air pollution monitoring (Wastine et al., 2022). The rugged design of the K96 sensor core combines highest compactness and low-power consumption with a unique multi-channel cell design, featuring the detection of up to three different gases simultaneously, including CO_2, methane (CH_4), nitrous oxide (N_2O), and water vapour (H_2O). The sensing platform allows the selection of the target gases as well as the concentration ranges, thus providing highly customizable gas sensor systems targeting application-specific gas monitoring settings. The sensor core comes with an implemented calibration model, and can address in real time any cross-sensitivity between the NDIR gas-sensing channels. The Senseair K96 sensor provide an immensely versatile sensing system while ensuring high sensing stability combined with high precision (<0.1 ppm for both CO_2 and N_2O, <0.5 ppm for CH_4). The K96 multi-gas sensor core offers a resilient sensor solution for the increasing demand of compact monitoring systems in the field of environmental monitoring at reasonable costs for medium-to-high volumes.

The optical design of the sensor is built according to the principal of the White cell with innovation of having early exit to the detectors that have shorter absorption path-length. Filters for these intermediate detectors are chosen so that they pass in the IR band of interest and simultaneously reflect further out of band portion of IR radiation to the detectors that follow.

Figure 1. Senseair K96 sensor

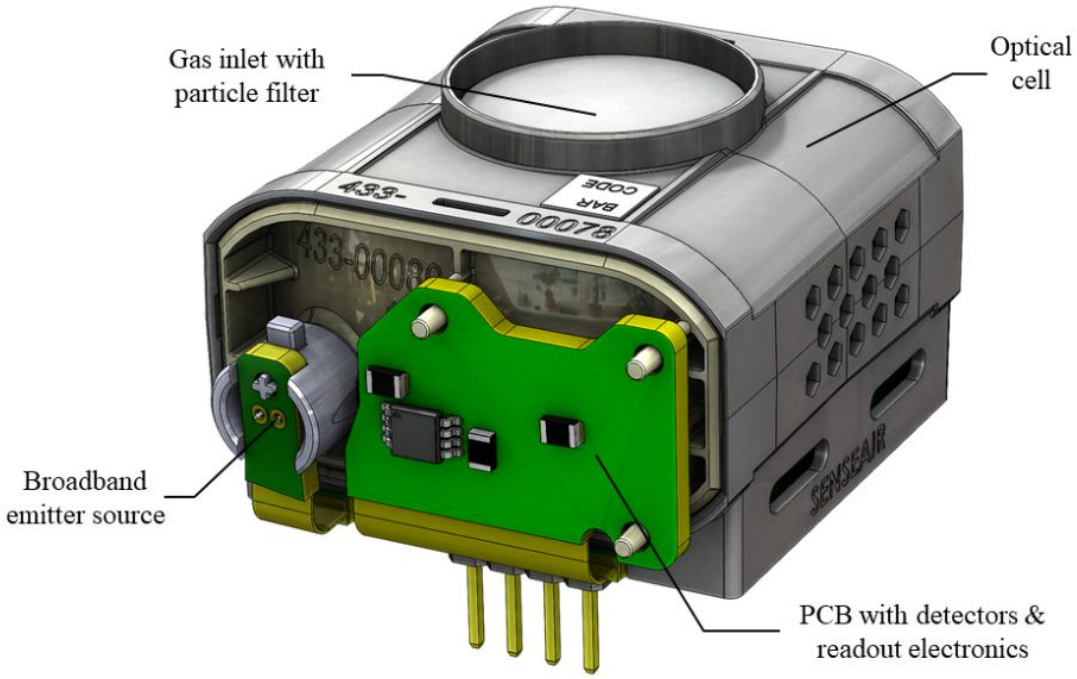

Source: Senseair, 2022.

The K96 Sensor relies on a novel patented optical concept, combining a multi-spectral and multi-optical path design in a single NDIR White-cell configuration. The Sensor Core, referred to the combined optical cell and readout electronics, houses a conventional incandescent emitter source featuring a broadband emission spectrum, an essential prerequisite for the multi-gas sensing capabilities. Furthermore, three individual wavelength selective detectors are mounted to the optical cell, separated by a complete propagation cycle between the spherical mirrors. Consequently, each of the wavelength-selective detectors is associated with a dedicated propagation path length within the White cell configuration. The broadband IR emitter injects the IR radiation into the multi-pass cell, where the IR spectrum is propagating between the opposing mirrors until reaching the detector of the Short Pass Length (SPL). The wavelength-specific optical filter in front of the detector allows the transmission of only the gas-specific IR wavelength range, whereas the remaining IR spectrum is reflected and propagates further within the Medium Path Length (MPL) and Long Path Length (LPL), respectively. By doing so, three separated NDIR gas-sensing channels are realized with varying optical path

lengths i.e., the Short Path Length with 24 cm, the Medium Path Length with 36 cm, and the Long Path Length with 48 cm, with the latter offering sub-ppm sensitivity. **Table 2** summarizes the currently available K96 configurations for monitoring gases that are showing a specific absorption band within the 1 μm to 6 μm wavelength range. Currently, the K96 sensor core is exploitable for measuring either CO_2, CH_4, or N_2O with sub-ppm resolution in combination with H_2O and CO_2 for monitoring with a 1 ppm resolution.

Table 2. List of the available gas-sensing configurations of the K96 sensor with respect to the different gas-sensing channels and resolutions.

LPL Channel 0.1 ppm Resolution	MPL Channel 1 ppm Resolution	SPL Channel 1 ppm Resolution
CO_2	H_2O	-
CH_4	H_2O	CO_2
N_2O	H_2O	CO_2

Source: Atmosphere 2022,13, 1789. https://doi.org/10.3390/atmos13111789. Creative Commons Attribution (CC BY) license

2.3 Integration into AirSensEUR sensor system

2.3.1 Presentation of AirSensEUR

AirSensEUR ([2]) is an Open Platform project developed by the JRC in Ispra (IT), in collaboration with Liberaintentio S.r.l (IT). The project aims to develop an open sensor platform targeted to accurate air quality measurements. Therefore, the AirSensEUR units are intended to be continuously developing prototypes including the most recent air quality monitoring technology, rather than to be complete and finalized products. The project started in 2015 and it's currently available at the 2nd hardware revision. Several units have been built and installed in multiple EU countries, mainly by universities and public/private research centres. Openness is not only limited to the hardware schematics but also includes the software running on the units and the calibration procedures implemented as a post-processing of the collected data.

AirSensEUR consists of a host capable to control several sensor shields (see **Figure 2**) through an AirSensEUR sensor bus. The host can send commands to sensor shields and retrieve sensor data. The host, built around the Arietta cpu (acmesystems.it), integrates functionalities shared by sensor shields including GPS positioning, Linux operating system and programming languages to control a list of I/O ports used by the shields (COM, USB, SPI, I2C, PWM …) with sufficient RAM, CPU computing capacity and a micro-SD storage up to 64 GB. The new version of the host controls a sensor bus capable to accept up to 15 sensor shields.

The data collected from AirSensEURs are stored locally into a sqlite3 formatted database and periodically sent to external server for offline post-processing and/or calibration. Storage technologies are based on standard database like InfluxDB and 52North SOS Db, MQTT and iFLINK APIs. The system is able to identify the data yet to be uploaded to the remote server, and sends only the required amount of data in the first time when the connection is available. Data is never deleted from the local database unless required. The local database may be accessed through SSH and/or deleted/backed-up to an external mass storage, if required, via simple Linux commands.

([2]) AirSensEUR website: www.airsenseur.org

Figure 2. Schematic diagram of the AirSensEUR sensor system

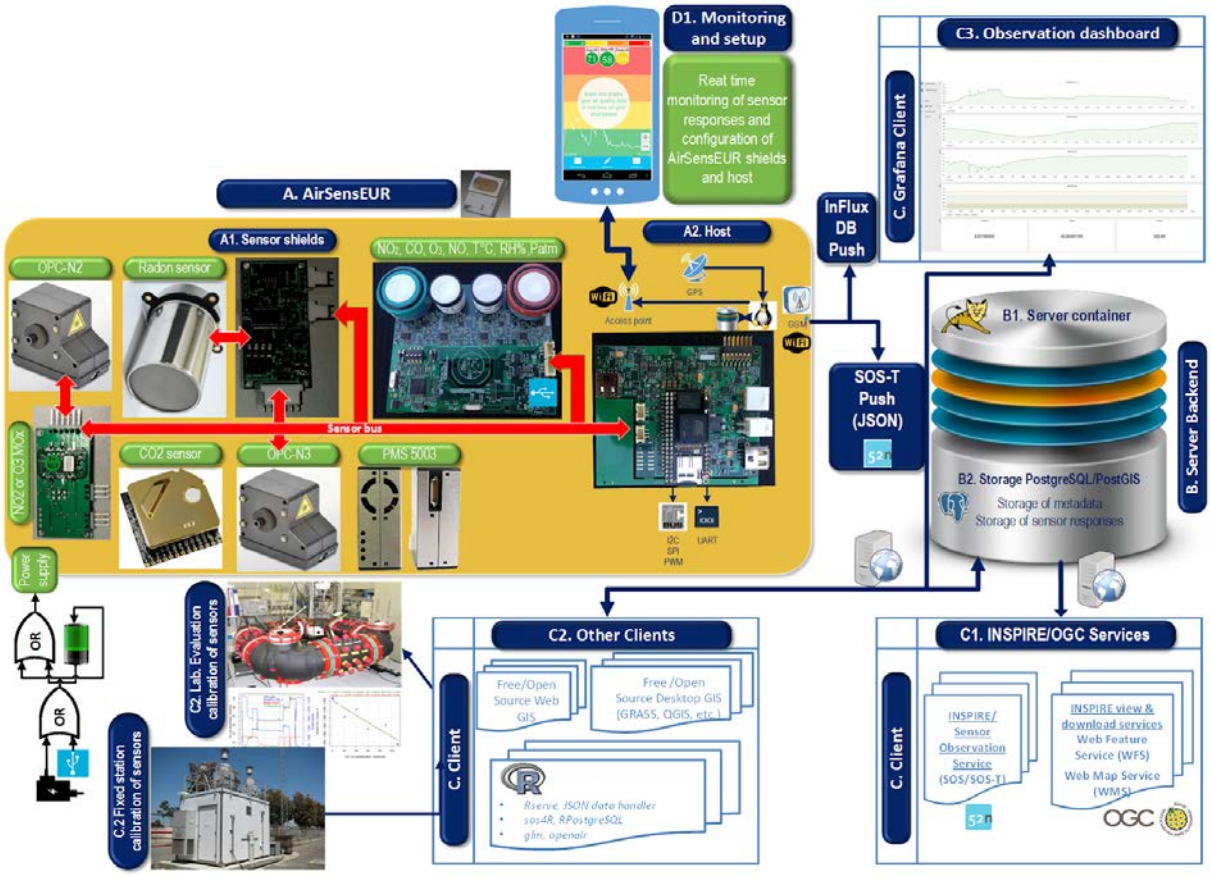

Source: LiberaIntentio S.r.l and JRC, 2022.

The collected data are transferred via GPRS/LTE or, optionally, via WiFi connections; all costs associated to transfer bandwidth and/or SIM for accessing to the mobile network are left to the final user and/or the local distributor.

AirSensEUR is made by a PTFE enclosure with a size of 26x22x10 cm and a weight of 2 kg, battery included. When installed outdoor, the PTFE enclosure needs to be inserted in a suitable stainless-steel protecting cover. The provided protective stainless-steel cover overall size is 35x32x30 cm except for the roof that's made by a 42x45 cm steel plate (see **Figure 3**). The horizontal mast may be fixed to a vertical pole through the provided toolset, or directly to a wall with non-provided screws. The overall weight, when mounted with the steel cover for outdoor install, is approx. 10 kg.

Figure 3. View of AirSensEUR system deployed at sampling site

Source: LiberaIntentio S.r.l and JRC, 2022.

2.3.2 Integration of Senseair K96 into AirSensEUR

A new temperature controlled chamber with a new electronic Shield (named Expansion Shield 2) was developed for accommodating the K96 CO_2/H_2O/CH_4 Senseair and ELT D300 sensors, see **Figure 4**.

The Expansion Shield 2 is an optional board targeted to fit Senseair K96 and ELT D300 sensors together for accurate CO_2 measurements. This shield is able to control a set of fans, heaters and Peltier cells in order to control a small chamber where the sensors are located. Controlling the temperature in the chamber reduces the uncertainty due to temperature and humidity variations. The Expansion Shield 2 fits on a custom PTFE enclosure, together with all the mechanical aspects to include a small insulated chamber made of extruded polystyrene (XPS), see **Figure 5**. Optionally, a Host board may be added in the same box for implementing a full working stand-alone unit. When not associated with a local Host board, the Expansion Shield 2 can be connected to an already available SensorBus through a 3 pin cable, as shown in **Figure 2**.

Figure 4. CO_2 sensor with temperature controlled elements and expansion shield (Expansion Shield 2)

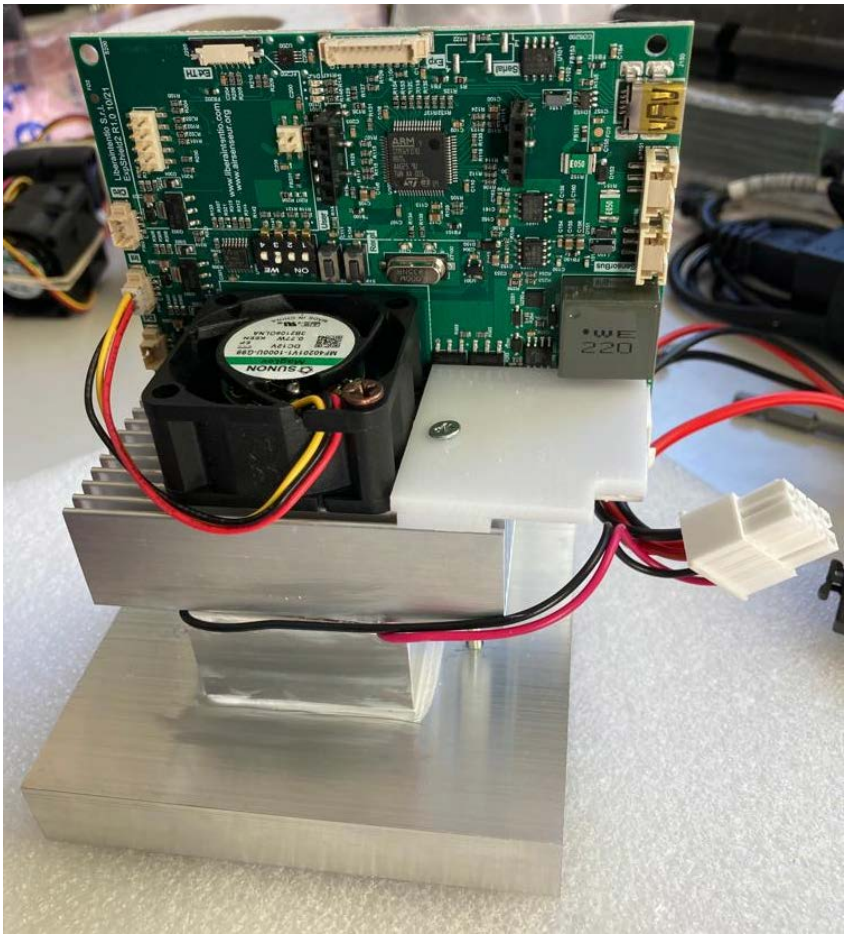

Source: LiberaIntentio S.r.l and JRC, 2022.

Figure 5. Installation of CO_2 sensors (K96 and ELT) on the expansion shield 2 into temperature controlled polystyrene chamber

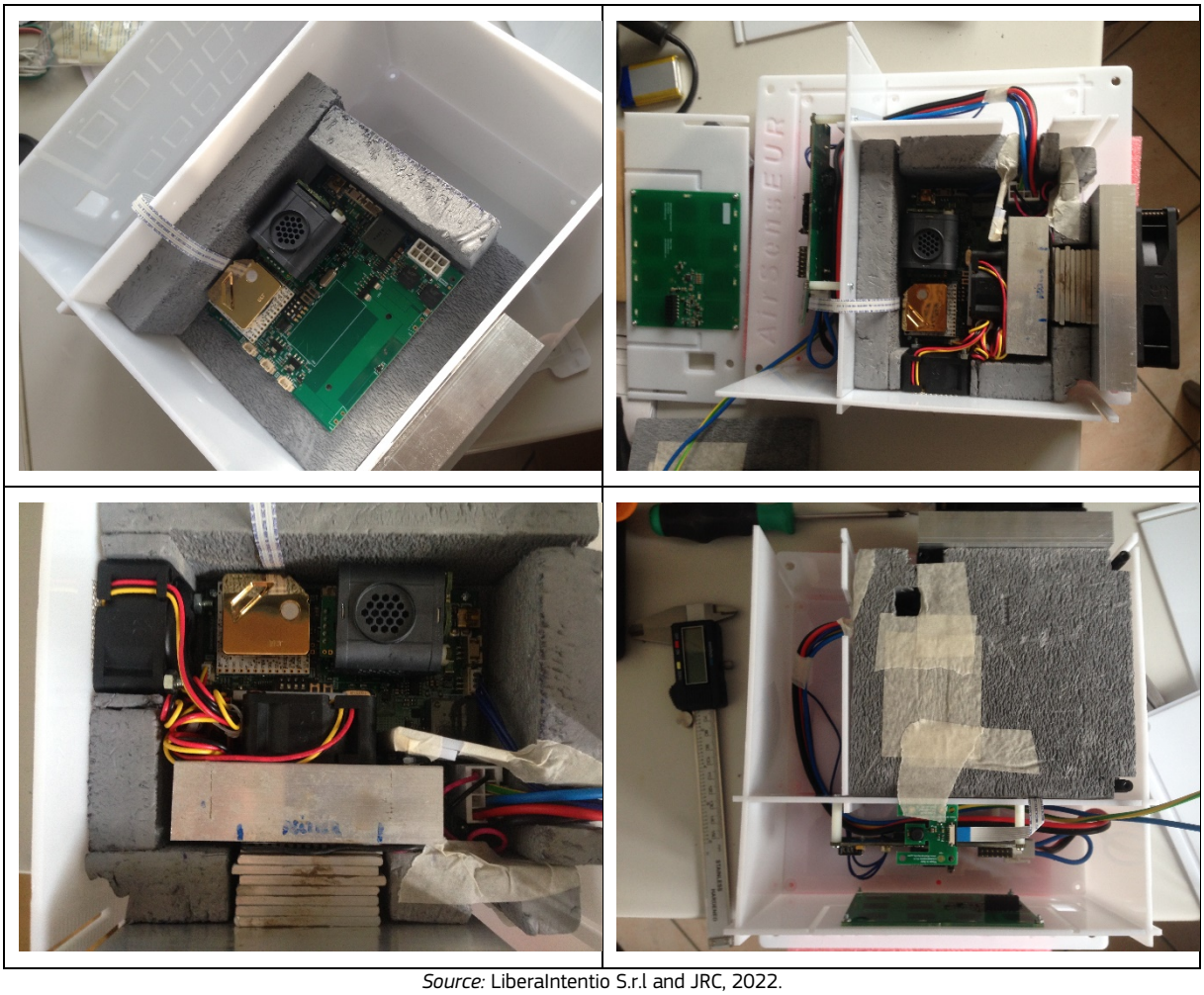

Source: LiberaIntentio S.r.l and JRC, 2022.

Table 3 gives the structure of AirSenSEUR data when downloaded from the InfluxDB server as a text file, including header names. In order to download AirSensEUR data, the ASE _App, developed at the JRC (Yatkin et al., 2022, Annex 2) was used. The ASE_App was configured so that the InfluxDB database returned minute data.

Table 3. List of parameters logged in the InfluxDB for the AirSensEUR equipped with temperature, humidity sensors (Sensirion SHT31), pressure sensors (BMP280) and CO2 sensors (ELT D300 and K96 sensors)

Manufacturer	Sensor model	INFLUX Name	Shiny equivalent	Unit	Comments
Sensirion	SHT31	SHT31TI	Temperature_int	C	Temperature inside AirSensEUR (inside measuring chamber)
Sensirion	SHT31	SHT31TE	Temperature	C	Temperature (Outside)
Sensirion	SHT31	SHT31HI	Relative_humidity_int	% RH	Humidity (Internal box)
Sensirion	SHT31	SHT31HE	Relative_humidity	% RH	Humidity (Outside)
Bosh Sensortech	BMP280	BMP280	Atmospheric_pressure	hPa	Atmospheric pressure (Outside)
ELT	D-300G-3V_2000PPM	D300	Carbon_dioxide	ppm	Carbon dioxide (Outside)
Analog Devices	ADT7470	TICHMBR	K96_Chamber_Temperature	C	CO_2 Internal chamber temperature at the center of the board
Analog Devices	ADT7470	TEHTSNK	Not defined	C	CO_2 Internal chamber temperature in the proximity of the external heatsink
Analog Devices	ADT7470	TIHTSNK	Not defined	C	CO_2 Internal chamber temperature in the proximity of the internal heatsink
Analog Devices	ADT7470	FEHTSNK	Not defined	rpm	External heatsink fan rotation speed
Analog Devices	ADT7470	FIHTSNK	Not defined	rpm	Internal heatsink fan rotation speed
Analog Devices	ADT7470	FACIRC	Not defined	rpm	CO_2 Internal chamber outlet air circulation fan rotation speed
AirSensEUR	ExpShield2	PELTV	Not defined	mV	Peltier cell actual voltage
AirSensEUR	ExpShield2	PELTC	Not defined	mA	Peltier cell actual current

AirSensEUR	ExpShield2	PSINV	Not defined	mV	Power supply actual voltage
AirSensEUR	ExpShield2	TUCBRD	Not defined	C	Microcontroller die temperature
AirSensEUR	ExpShield2	PIDH	Not defined	%	Power applied to the heaters in the CO_2 internal chamber
AirSensEUR	ExpShield2	PIDC	Not defined	%	Power applied to the Peltier cooler cell in the CO_2 internal chamber
Senseair	K96	LPLCPC	K96_Methane	ppm	Concentration for the K96 LP channel
Senseair	K96	SPLCPC	K96_Carbon_dioxide	ppm	Concentration for the K96 SP channel
Senseair	K96	MPLCPC	K96_Methane	ppm	Concentration for the K96 MP channel
Senseair	K96	PSEN0	K96_Atmospheric_pressure	hPa	Atmospheric pressure (K96)
Senseair	K96	TNTC0	K96_NTC0	C	Temperature measured by the K96 NTC0 channel
Senseair	K96	TNTC1	K96_NTC1	C	Temperature measured by the K96 NTC1 channel
Senseair	K96	TUCDIE	Not defined	C	Temperature of the K96 internal microcontroller die
Senseair	K96	RH0	K96_Relative_humidity	% RH	Humidity measured by the K96 internal BME280 sensor
Senseair	K96	TRH0	K96_Temperature	C	Temperature measured by the K96 internal BME280 sensor
Senseair	K96	ERRST	K96_Error	bitfield	K96 internal error register bitfield (no average is performed on this channel, but the register value received with the last sample)

Source: JRC and LiberaIntentio s.r.l, 2022.

3 Carbon dioxide reference data

The CO_2 reference measurements were obtained using a Picarro G2404 analyser placed at the JRC Atmospheric Observatory where the AirSensEUR CO_2 sensor system was deployed 50 cm away.

3.1 Principle of operation of the Picarro G2401

The Picarro G2401 analyser used in this study (serial number 3551-CFKADS-2357) measures atmospheric concentrations of CO_2, CH_4, carbon monoxide (CO) and H_2O every 5 seconds through the wavelength-scanned cavity ring-down spectroscopy (WS-CRDS). The heart of the WS-CRDS analyser is the optical cavity, a small flow cell with a volume of around 35 cm^3 and an effective optical path length of 20 km. Operationally, light from a single-frequency laser enters the cavity where three mirrors reflect the laser light as shown in **Figure 6**. When the laser is on, the light intensity inside the cavity increases quickly. However, a small amount of the laser light is transmitted through the mirror closest to the photodetector, which turns the incident light into a signal linearly correlated to the light intensity in the cavity. When the photodetector signal reaches a threshold, the laser is turned off. At this point most of the light remains trapped within the cavity for a long time, travelling along an effective path length of tens of kilometres through the air sample. Since the mirrors have a 99.999% reflectivity, the light inside the cavity steadily leaks out of the cavity. The intensity of the light reaching the detector decreases exponentially in time, until it reaches zero. This decay, or "ring-down," is measured in real time by the photodetector.

The time it takes to ring-down is inversely related to the total optical loss in the cavity, including the strength of molecular absorption at a given wavelength of light. For an empty cavity, the time required for the intensity to decrease by a given percent is determined solely by the reflectivity of the mirrors. A cavity containing gas that absorbs light will have a shorter ring-down time than an empty cavity. As the light circulates in a cavity with a gas sample, the molecular absorption by the gas results in a decrease of the light intensity.

Determining absorption intensity at a specific wavelength requires comparing the ring-down time of an empty cavity to the ring-down time of a cavity that contains gas. The Picarro G2401 instrument gathers measurements from an “empty” cavity by switching the light to wavelengths that are not absorbed by the target molecules. The analyser subsequently measures ring-down times at wavelengths that are absorbed by the target gas. The analyser automatically and continuously compares these two types of ring-down times, and the software uses those comparisons to calculate absorption intensities.

Figure 6. Schematic of the Picarro G2401 analyser cavity. Motion of laser light is represented by the dark-orange path

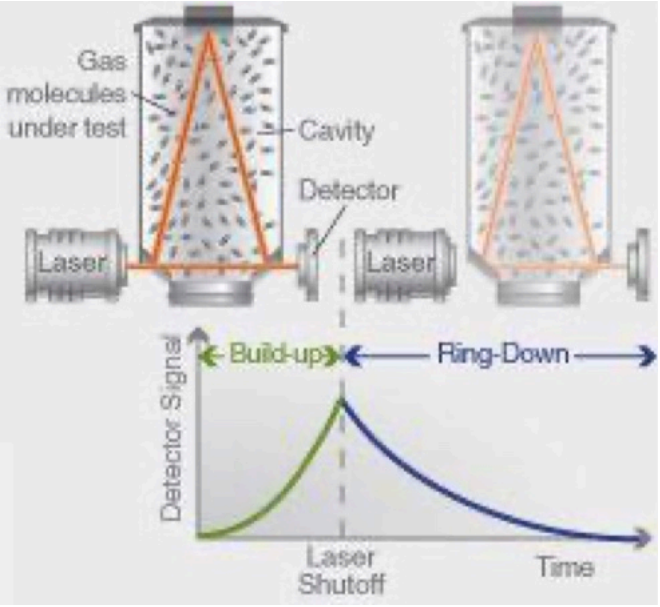

Source: www.picarro.com

Plotting the absorbance at each measured wavelength generates an optical spectrum. This spectrum contains absorbance peaks that are unique to each molecule in the sample. The height of a particular absorption peak

is proportional to the concentration of a molecule that generates the signal. The height of the peak is calculated by subtracting the maximal absorbance from the baseline absorbance.

The high spectral precision of Picarro G2401 is mainly related to the proprietary wavelength monitor (WLM) and the precise temperature and pressure control in the sample cavity. The WLM measures the absolute laser wavelength to a precision that is a few orders of magnitude narrower than the spectral linewidth. The laser is continuously tuned to known wavelengths measured by the WLM. Moreover, the cavity temperature is locked at 45 °C with a very small variability allowed (lower than 20 m °C) through the thermal insulation system and a solid-state heating system locked to the output of a thermal sensor. Sample pressure inside the cavity is continuously measured with a high precision pressure transducer. The sensed pressure is used in a feedback loop to control the opening of proportional valves, which adjust the inlet and outlet gas flow of the cavity. In this way, the pressure of Picarro G2401 instrument is stabilized to 140 Torr with an allowed variability of 0.152 Torr. The measurement and control of laser wavelength, sample pressure and temperature allow the Picarro G2401 analyser to reach ppbv to pptv sensitivity and a long term (30-day) measurement drift at the ppbv level. This enables the Picarro G2401 instrument to be operated for several months without requirement of any re-calibration.

In this study, the Picarro G2401 was successfully tested at the ICOS Atmosphere Thematic Centre (https://icos-atc.lsce.ipsl.fr/) prior to usage. The tests were carried out to evaluate the performance of the instrument and its compliance with requirements for atmospheric observations in the ICOS network (for more details see the link: https://box.lsce.ipsl.fr/index.php/s/YKxksYdSoVUtPPr). **Figure 7** shows the certificate of compliance issued by the ICOS Atmosphere Thematic Centre that contains the results of all tests.

Figure 7. ICOS compliance certificate for the Picarro G2401 analyser used in this study. The certificate reports the results of performance tests carried out at the Metrology Laboratory of the ICOS Atmosphere Thematic Centre (ATC).

ICOS Atmosphere Thematic Centre

Certificate of Compliance

Certificate n°: ATC-ML-IT-CoC-142-1.0_IT_1075
Issued to the instrument 1075 (PICARRO 3551-CFKADS-2357)

Tested by: D. Desbree et A. Platon from 2020-02-18 to 2020-06-17

Tests	CO_2			CH_4			CO			Test definition
	ICOS Spec	ATC test results	Status	ICOS Spec	ATC test results	Status	ICOS Spec	ATC test results	Status	
Minute CMR (1σ, [ppb])	<50	**6**	Pass	<1	**0.04**	Pass	<2	**0.69**	Pass	Measure continuously a tank filled with dry natural air during at least 25 hours. Look at data dispersion (1σ) for minute average. First hour not taken into account (stabilization time). No calibration applied.
Hourly CMR (1σ, [ppb])	<25	**3**	Pass	<0.5	**0.02**	Pass	<1	**0.11**	Pass	Measure continuously a tank filled with dry natural air during at least 25 hours. Look at data dispersion (1σ) for hourly average. First hour not taken into account (stabilization time). No calibration applied.
LTR (1σ, 10 min avr raw data, [ppb])	<50	**7**	Pass	<0.5	**0.02**	Pass	<1	**0.34**	Pass	Measure alternatively over 72 hours a tank filled with dry natural air for 30 minutes and 270 minutes of ambient air (not dry). For each period of tank measurement, calculate a mean value (last 10 minutes). Look at the dispersion (1σ) of the mean values. No calibration applied.

ICOS status: COMPLIANT with the ICOS specifications [AD2]

Date issued: 2020-06-17

Olivier Laurent
Metrology laboratory manager
ICOS ATC
France

Source: JRC, 2022

3.2 Air sampling system and calibration

Air samples analysed by the Picarro G2401 instrument are collected at 10 m above ground using ½" (OD) Synflex tube at a flow rate of ~10 L min^{-1} (see **Figure 8**). The sampling line is equipped with a vacuum pump (KNF N86KN), and two different particulate filters: a Pall HEPA Capsule Versapor filter at the inlet, and a filter with nominal pore sizes of 7 µm (model Swagelok, SS-8TF-7).

A small air flow (around 0.2 L min^{-1}) is diverted from the main line toward the Picarro G2401 instrument using a dedicated vacuum pump (model Vacuubrand, MD1) located downstream to the analyser. The Picarro instrument controls the rotary valve (model Valvo Vici, EMT2SD12MWE) that is used to select the air flow directed to the analyser. This valve is mainly used to select the gas cylinders analysed by the Picarro G2401 during the calibration event, and during ambient measurements, air is continuously sampled at only one level, that is 10 m above ground level. Three gas cylinders, with CO_2 concentration in the range of 409 – 471 ppm, are used for calibration, and they are measured in a row for 30 minutes each. This sequence is repeated twice at each calibration time, but only the second one is retained for further calculations. The last five minutes of each cylinder measurements are used to calculate the average concentration of CO_2 corresponding cylinder. Then, the mean concentrations of three calibration cylinders are plotted against their assigned values, and the calibration equation is determined by linear least square fitting.

The assigned CO_2 concentrations of calibration cylinders have been attributed by the ICOS Central Analytical Laboratories (CAL) using the World Meteorological Organization (WMO) scales maintained by the Central Calibration Laboratory at NOAA-ESRL (https://gml.noaa.gov/ccl/scales.html). **Table 4** reports the assigned CO_2 values of the cylinders used to calibrate the Picarro G2401. The calibration scale for CO_2 is the WMO-CO2-X2019.

The three calibrations were performed in the period of December 2021 and November 2022. As shown in **Figure 9** (top panels), the three calibration equations did not change significantly through the three calibration events. Moreover, the stability of the instrument response has been evaluated through the difference between the assigned cylinder concentration and the measured value during a specific calibration event. This difference is a good indicator to detect any drift of the analyser. The results reported in **Figure 9** (bottom panel) did not show any significant drift of the Picarro analyser during the period covering the three calibrations events (around 11 months). Moreover, the measured concentrations for a specific cylinder changed less than 0.06 ppm between consecutive calibrations.

Figure 8. Sampling and distribution system diagram for measurement of atmospheric CO_2 concentrations through the Picarro G2401 analyser

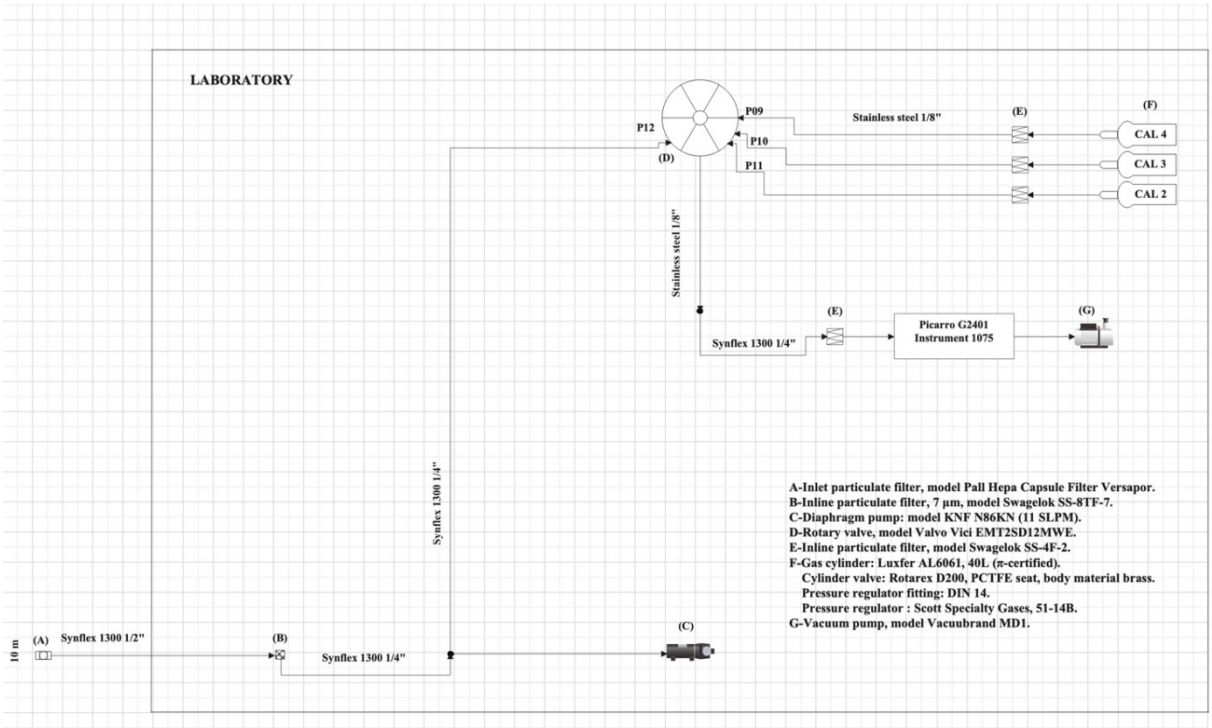

Source: JRC, 2022

Figure 9. Top panels: measured CO_2 concentrations of the three calibrations cylinders against the assigned tank values for the three calibration events (on 2021-12-21, 2022-07-20, and 2022-11-03). Dashed-dot line represents the calibration equation estimated through linear least square fitting. Bottom panel: the difference between measured CO_2 concentration of a specific calibration cylinder and the assigned CO_2 concentration for the same cylinder, for a specific calibration event. Error bars denote the standard deviation of the measured value.

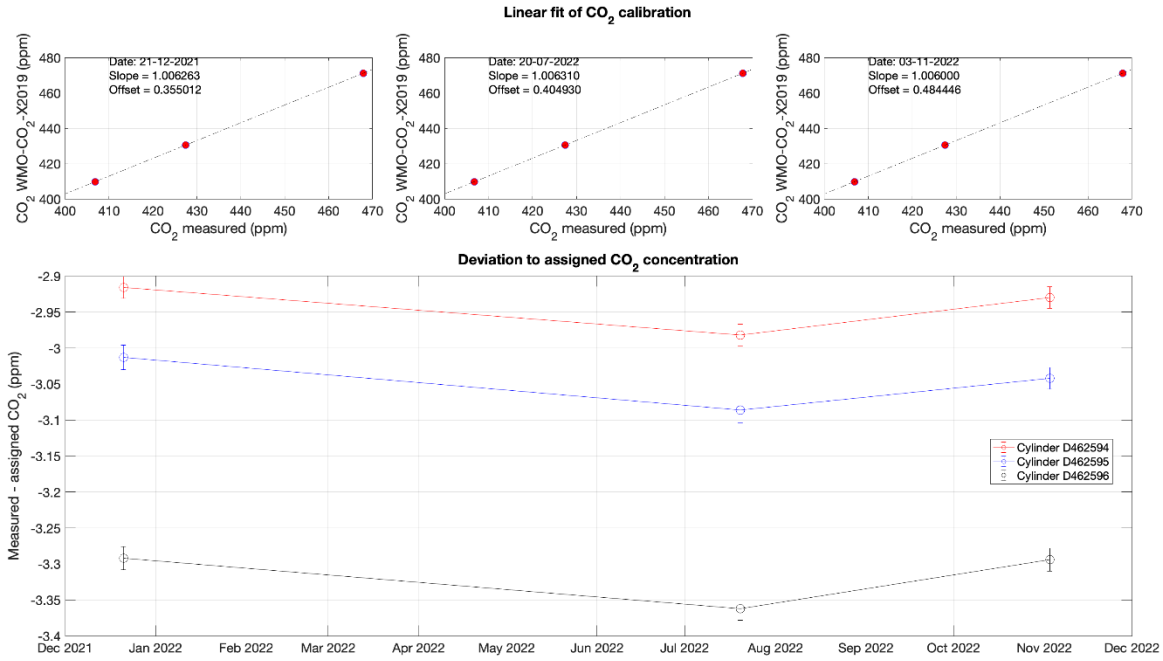

Source: JRC, 2022

Table 4. CO_2 concentration in the cylinders used for the calibration of Picarro G2401. Uncertainty of the assigned concentrations is reported as repeatability. The calibration scale used is the WMO-CO2-X2019.

Cylinder name	Cylinder s/n	CO_2 (ppm)	Repeatability (ppm)	Scale
CAL 2	D462594	409.78	0.015	WMO-CO2-X2019
CAL 3	D462595	430.48	0.023	WMO-CO2-X2019
CAL 4	D462596	471.19	0.025	WMO-CO2-X2019

Source: JRC, 2022.

3.3 Reference data structure

The reference measurements of Picarro G2401 were transmitted as text daily files (.dat). The periodicity of data logging was 5 s with one row for each measurement. All daily data files were concatenated into one csv file with one row of minute averaged measurement. **Table 5** shows the headers of the data contained into the csv file. All data rows showing an Alarm_status equal to 1 were discarded prior to averaging to minutes values.

All the Picarro raw wet CO_2 measurements (CO2_Sync) were corrected for calibration drift (column CO2_Sync_Cal) using the following scheme:

- for the data between the 1st and 2nd calibrations, the CO_2 measurements were corrected using a linear function with the slope and intercept of the 1st calibration (see **Figure 9**),
- for the data between the 2nd and 3rd calibrations, the CO_2 measurements were corrected using a linear function with the slope and intercept of the 2nd calibration (see **Figure 9**),
- for the data after the 3rd calibration, the CO_2 measurements were corrected using a linear function with the slope and intercept of the 3rd calibration (see **Figure 9**).

Table 5. The header names of parameters included into the reference data file of Picarro G2401 instrument.

Parameter	**Description**
date	Date time in POSIX format with UTC time zone
ALARM_STATUS	Boolean values, 1: data is not valid and 0 data is valid
CO_sync	Raw CO Picarro G2401 measurements in ppm (dry CO)
CO2_sync	Raw CO_2 Picarro G2401 measurements in ppm (wet CO_2)
CO2_dry_sync	Raw CO_2 Picarro G2401 measurements corrected for water vapour in ppm (dry CO_2)
CH4_sync	Raw CH_4 Picarro G2401 measurements in ppm (wet CH_4)
CH4_dry_sync	Raw CH_4 Picarro G2401 measurements corrected for water vapour in ppm (dry CH_4)
H2O_sync	Raw H_2O Picarro G2401 measurements in ppm (wet CH_4)
CO2_sync_cal	Calibrated CO_2 Picarro G2401 measurements in ppm (calibrated wet CO_2)
CH4_sync_cal	Calibrated CH_4 Picarro G2401 measurements in ppm (calibrated dry CH_4)

Source: JRC, 2022.

4 Field experiments

The 1st AirSensEUR prototype, called Asdebug, equipped with the temperature controlled chamber where the CO_2 sensors are installed was deployed at the JRC Atmospheric Observatory station on December 4th, 2021. The experiment is still on going. The reference CO_2 measurements are performed using a Picarro G2401 analyser (see section 3). The current report presents the sensor CO_2 measurements for the K96 LCS of this AIrSensEUR since it is the only unit collecting data for a long time.

The Asdebug AirSensEUR always returned the sensor data when it was switched-on. However, two major power outages occurred at the JRC observatory since the unit was switched-on. The 1st one was on 2022-02-05 12:44 and the unit was restarted on 2022-02-14 12:21. The 2nd one occurred on 2022-09-07 22:50 and the unit was restarted on 2022-09-16 16:20. In addition, the AirSensEUR was switched off between 2022-10-14 14:30 and 2022-10-17 15:35 due to many brown marmorated stink bugs clogged the ventilator used to cool down the Peltier cell of temperature controlled chamber with a high risk to damage to the electronic.

The calibration of sensor was performed using sensor's and reference data in minute resolution. The agreement between predicted sensor and reference data was checked using hourly data resolution. Both the wet sensor (see SPLCPC in **Table 3**) and reference (see CO2_sync_cal in **Table 5**) values were used for the data treatment using the ASE _App, using built in functionalities (Yatkin et al., 2022).

Five other AirSensEUR sensor systems equipped with CO_2 sensors were prepared but could not be finalised in the planned time due to electronic components shortage during the COVID pandemic. Finally they were deployed at the JRC Atmospheric Observatory station at the end of September, beginning of October 2022 (see **Table 6**).

Table 6. List of AirSensEUR sensor systems equipped with temperature controlled CO_2 sensors installed at the JRC Atmospheric Observatory station

AirSensEUR IDs	Starting date	IDs of ELT D300 sensors	IDs of Senseair K96 sensors	Senseair K96 sensors, channel LPL	Senseair K96 sensors, channel MPL	Senseair K96 sensors, channel SPL
Asdebug	2021-12-04	MCXXX1	01:00:A2:E8	CH_4	H_2O	CO_2
400AF0	2022-10-03	MC02-041	01:00:A2:EE	CH_4	H_2O	CO_2
40499H	2022-10-03	MC02-039	01:00:A3:00	CO_2	H_2O	
4049A6	2022-09-29	MC02-040	01:00:A2:1D	CO_2	H_2O	
652D1F	2022-10-03	MC02-038	01:00:A2:FF	CO_2	H_2O	
652D37	2022-09-29	MC02-037	01:00:A2:E7	CH_4	H_2O	CO_2

Source: JRC and LiberaIntentio s.r.l, 2022.

4.1 General calibration principles and equations

In the following sections, the calibration models of the CO_2 sensor will be presented. The calibration models are the combined responses of both sensor and electronics embedded into the AirSensEUR sensor system.

The overall effects of covariates including the pollutant of interest on sensor responses can be described by Equation 1 that is referred to the calibration model:

$$\widehat{R_t} = a_0 + a_1\, x_t + \sum_{j=2}^{n-1} a_j\; Z_{j,t}^{m_j} \qquad \text{Equation 1}$$

Where:

— $R_{i,t}$ is the time series of raw sensor response in raw units at time t with a chosen time resolution (e.g., 1 min) over the whole calibration period (e.g., 2 weeks); $\widehat{R_t}$ is the sensor response estimated using Equation 1.

— n is the number of coefficients in Equation 1 from a_0 to a_{n-1}.

— a_0, a_1 and a_j with j between 2 and n-1 are the coefficients of the model; we refer to the set of coefficients as a_n where n ranges between 0 and n-1.

— x_t is the time series of reference measurements at time t, in units of the reference measurements, ppm;

— $Z_{j,t}$ are the time series of covariates having an effect on R_t at time t, in addition to x_t, with exponent m_j.

The degrees of exponents m_j are generally equal to 1. The main assumption of Equation 1 is that the effect of all covariates on R_t are additive.

The calibration models were initially established by fitting a model using Equation 1. Once sensors are calibrated, unknown pollutant concentrations at any time are computed using Equation 2, hereinafter called prediction:

$$\widehat{x_t} = \frac{R_t - (a_0 + \sum_{j=2}^{n-1} a_j \ Z_{j,t}^{m_j})}{a_1} \qquad \text{Equation 2}$$

where $\widehat{x_t}$ is the predicted CO_2 concentration at time t in the same unit as x_t.

4.2 Calibration of sensor

Among the whole data series between 2021-12-21 and 2022-10-14, sub-periods were selected to calibrate the CO_2 sensors simulating scenarios of calibration and examine the period yielding the best calibration:

— Typical periods for winter, between 2022-02-14 and 2022-02-28

— Long winter and spring periods before the high summer temperature, between 2022-02-14 and 2022-07-06

Table 7 gives basic statistics for several calibrations and predictions of the Senseair K96 sensor data by applying the calibration function using Equation 2 where R^2 is the coefficient of determination and RMSE is the root mean square error. The first column of Table **7** gives a hyperlink to an section number where for each calibration/prediction, showing a set of plots with the calibration scatterplots and time series, the prediction time series and drift, and a correlation matrix with residuals (predicted sensor – reference) versus water vapour, atmospheric pressure and relative humidity in the Senseair K96 sensor (K96 Water vapour, K96 Atmospheric pressure, K96 relative humidity), SPLSPC the raw adjusted wet CO_2 sensor data (SPLCPC), the Picarro CO_2 data (Ref) and the predicted CO_2 sensor data (SPLCPC Cal).

Table 7. Calibrations of Senseair K96 CO_2 sensors at the JRC Observatory. All units are in ppm.

	Calibration, Sensor vs Reference, minute data				Prediction, Sensor vs Reference, hourly data				
	Start	**End**	**R^2**	**Calibration model**	**Start**	**End**	**Slope/int.**	**RMSE**	**R^2**
4.2.1	2022-02-14	2022-02-28	0.97	R_{CO2} = -2.641+ 1.008 CO_2	2021-12-21	2022-10-14	0.79/115	25	0.58
4.2.1	2022-02-14	2022-07-06	0.74	R_{CO2} = 37.812+ 0.99 CO_2	2021-12-21	2022-10-14	0.81/76	25	0.58
4.2.1	2022-02-14	2022-07-06	0.74	R_{CO2} = 37.812+ 0.99 CO_2	2021-12-21	2022-07-06	0.85/43	15.6	0.80
4.2.2	2022-02-14	2022-07-06	0.95	R_{CO2} = -4.19+ 0.97 CO_2 +0.00202 K96_H_2O	2021-12-21	2022-10-14	1.02/2.6	14	0.84
4.2.2	2022-02-14	2022-07-06	0.98	R_{CO2} = -593.11+ 0.95 CO_2 +0.00223 K96_H_2O +0.601 K96_Press	2021-12-21	2022-10-14	0.98/17.3	13.3	0.88
4.3	2022-04-01	2022-06-01	0.99	R_{CO2} = -557.2+ 0.951 CO_2 -0.410 K96_Temp +0.577 K96_Press+0.00192 K96_H_2O	2021-12-21	2022-10-14	0.94/36.6	14.7	0.85

Source: JRC, 2022.

4.2.1 Linear models

The quantile regression (Koenker et al., 2018) was used for fitting a linear line.. It has the advantage of honouring the median, or any other percentile, of sensor datasets rather than their mean. The LCSs are likely to produce outliers occasionally, thus, quantile regression is preferred over Ordinary Least Square linear regression (OLS) (Draper and Smith, 1998), thanks to being more robust and less sensitive to outliers.

The calibration with quantile regression between 2022-02-14 and 2022-02-28 yielded a perfect calibration model with the metrics close to the ideal values, namely slope, intercept and R^2 being respectively close to unity, zero and 1. (see **Figure 10**). However, **Figure 11** shows that a linearly increasing bias between predicted sensor and reference data started sometime between April and May 2022. **Figure 12** shows that the residual is strongly associated firstly with water vapour and secondly with the relative humidity in the sensor measuring chamber while it is not associated with ambient pressure in the sensor chamber.

Figure 10. SenseAir K96 sensor, calibration using quantile regression between 2022-02-14 and 2022-02-28. Up: scatterplot of calibration, data in minute resolution; down: time series of minute data. (predicted sensor in blue and reference in red lines).

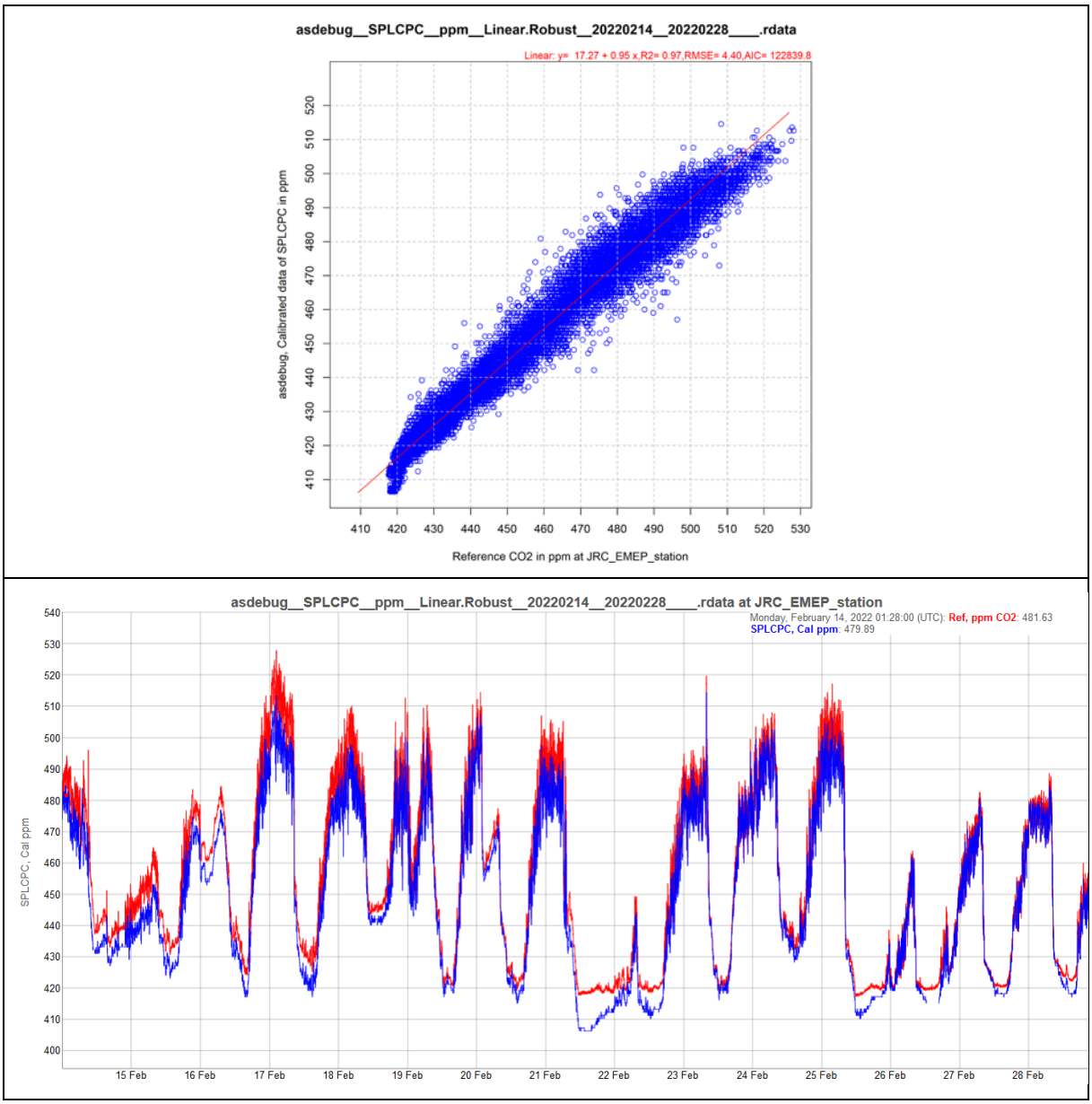

Source: JRC, 2022

Figure 11. Up: time series of hourly sensor data predicted using the quantile regression calibration model (in blue) and reference (in red); down: daily residuals (drift). The prediction period is between 2021-12-21 and 2022-10-14.

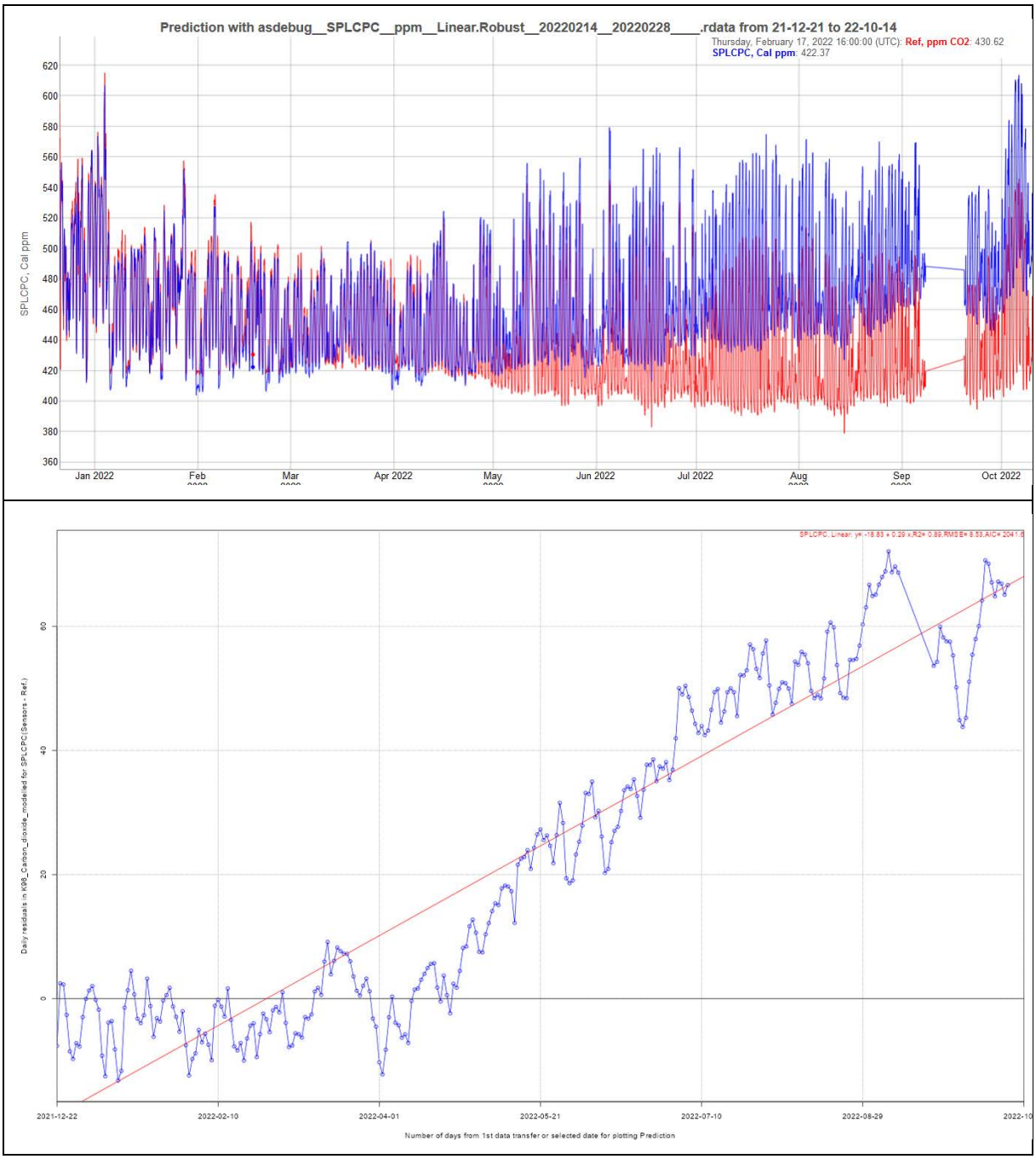

Source: JRC, 2022

Figure 12. SenseAir K96 sensor, calibrated using quantile regression between 2022-02-14 and 2022-02-28. Plot of correlation matrix with residuals of hourly predicted data versus water vapour, atmospheric pressure relative humidity and temperature in the SenseAir K96 measuring chamber (K96 Water vapour, K96 Atmospheric pressure, K96 Relative humidity and K96 Temperature), the raw wet CO_2 sensor data (SPLCPC), the Picarro CO2 data (Ref) and the predicted CO2 sensor data (SPLCPC Cal). The period is between 2021-12-21 and 2022-10-14.

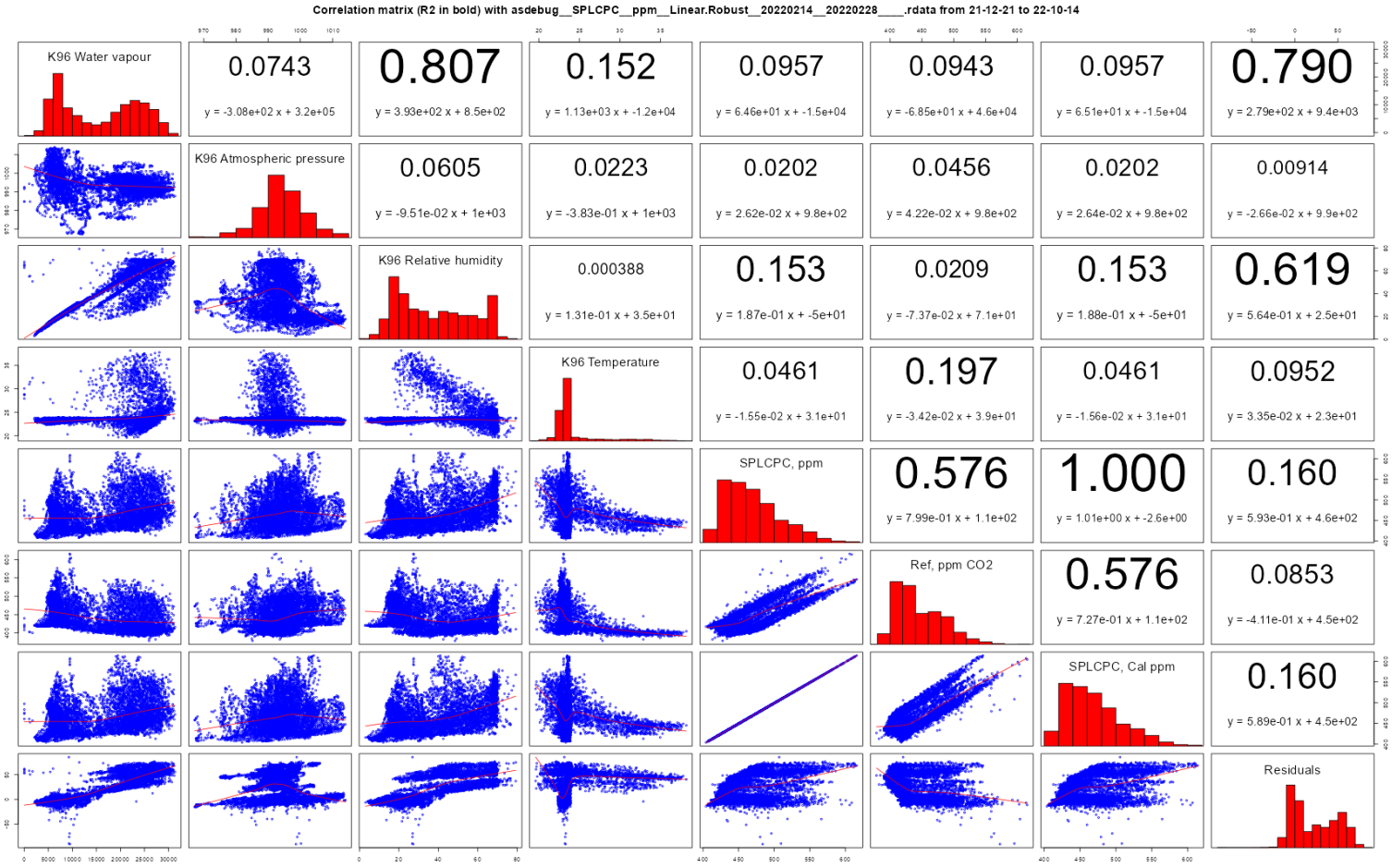

Source: JRC, 2022

In the second attempt, we enlarged the calibration period to be between 2022-02-14 and 2022-07-06. The results are given in **Table 7**. The major results are a worsened R^2 of the calibration data due to a significant sensor drift within the calibration period (**Figure 13**), an increase in the intercept of the calibration line, an identical R^2 and RMSE for the hourly predicted sensor data and similar drift more balanced around zero (see **Figure 14**). Finally, **Figure 15** shows a residuals matrix having similar pattern to the one of calibration between 2022-02-14 and 2022-02-28 shown in **Figure 12**, both revealing strong effects of water vapour and relative humidity.

Based on the aforementioned findings, it is clear that a simple linear model relying on the wet CO_2 sensor wouldnot provide predicted sensor data in good agreement with the wet CO_2 reference data from the Picarro analyser.

Figure 13. SenseAir K96 sensor, calibration using quantile regression between 2022-02-14 and 2022-07-06. Up: scatterplot of calibration in minute resolution; down: time series of minute data. (predicted sensor in blue and reference in red lines).

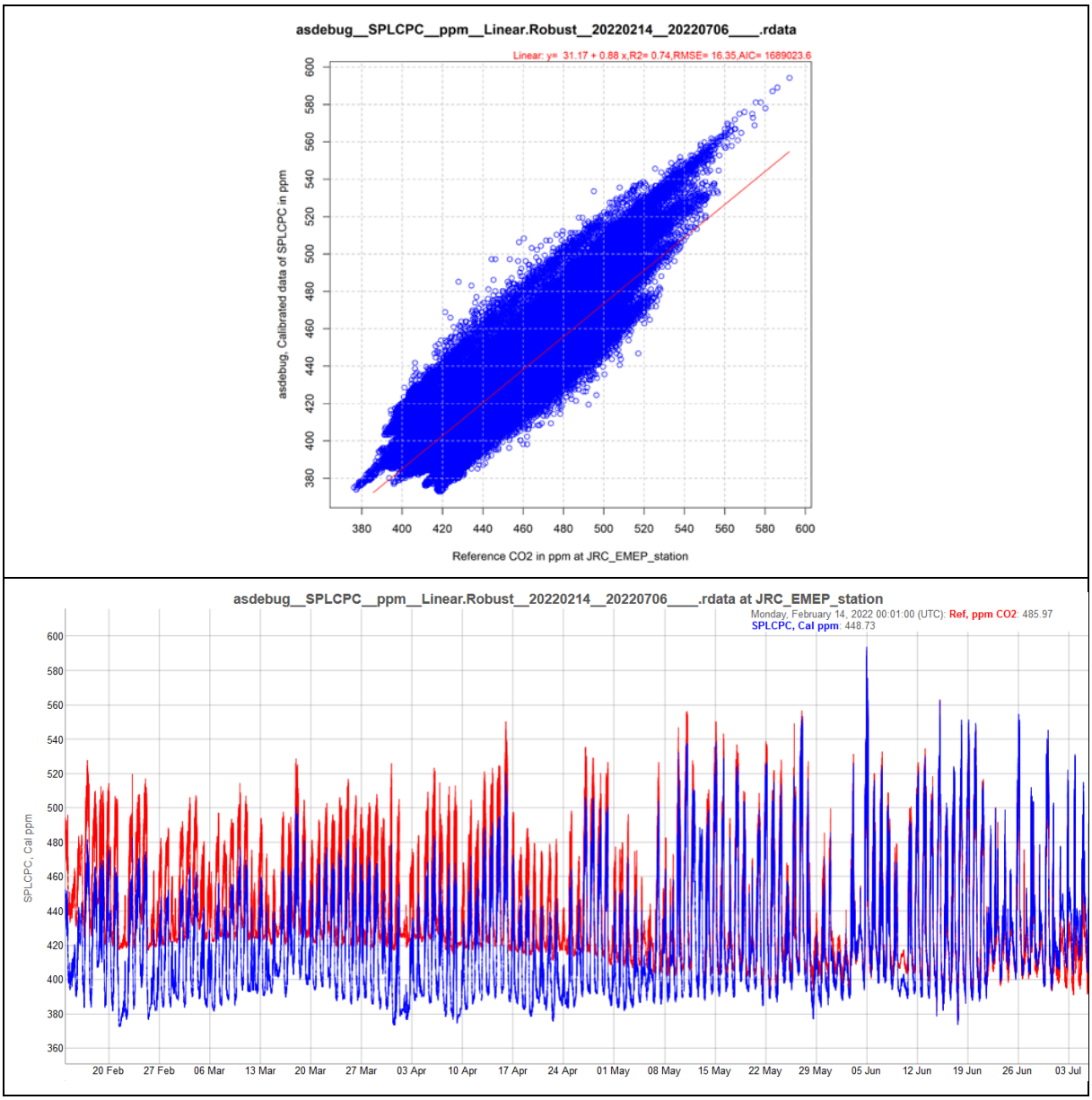

Source: JRC, 2022

Figure 14. Up: time series of hourly sensor data predicted using the quantile regression calibration model (in blue) and reference (in red); down: daily residuals (drift). The prediction period is between 2021-12-21 and 2022-10-14.

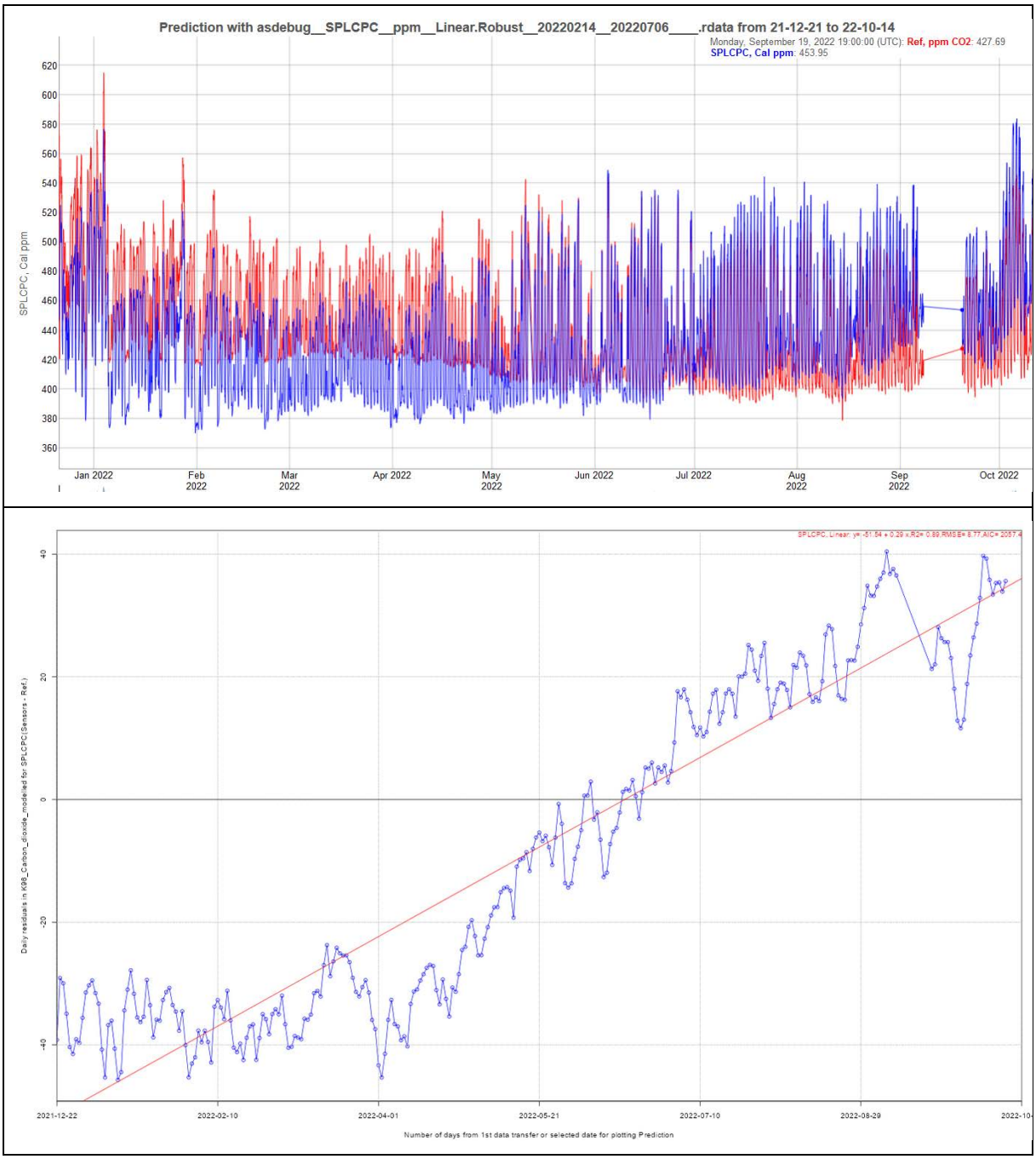

Figure 15. SenseAir K96 sensor, calibrated using quantile regression between 2022-02-14 and 2022-07-06. Plot of correlation matrix with residuals of hourly predicted data versus water vapour, atmospheric pressure, relative humidity and temperature in the SenseAir K96 measuring chamber (K96 Water vapour, K96 Atmospheric pressure, K96 relative humidity and K96 Temperature), the raw CO_2 sensor data (SPLCPC), the Picarro CO_2 data (Ref) and the predicted CO_2 sensor data (SPLCPC Cal). The data period is between 2021-12-21 and 2022-10-14.

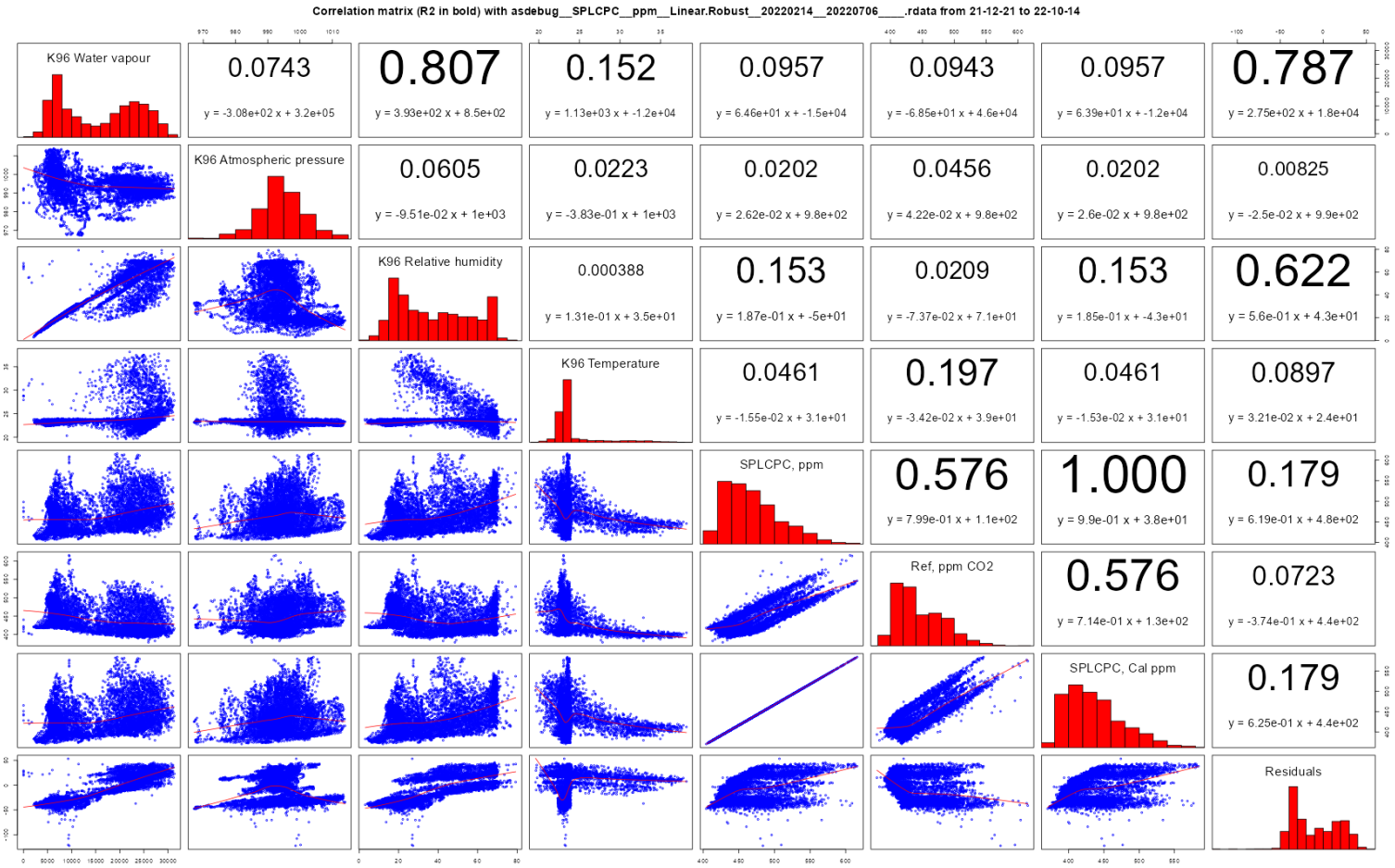

Source: JRC, 2022

4.2.2 Multiple linear models

Figure 12 and **Figure 15** show strong effects of water vapour and relative humidity on the CO_2 sensor measurement. However, as both water vapour and relative humidity in the sensor measuring chamber are strongly correlated (R^2 = 0.807 in **Figure 12**) , it is not convenient to add both into a multiple linear model without the risk of estimating the coefficients of the model (a_j) and their standard deviations incorrectly. Therefore, as the water vapour shows the strongest correlation with residuals, it was firstly retained alone for calibration using Equation 1. Subsequently, the residuals of predicted data, computed using Equation 2 were examined to evidence any correlation with other covariates. It is noteworthy that the coefficient of water vapour in the calibration model includes both effects of water vapour and relative humidity that cannot be distinguished since these two parameters are strongly correlated.

The calibration and prediction results for the multiple linear regression model with K96 water vapour between 2022-02-14 and 2022-07-06 are given in **Table 7**. The R^2 of calibration (0.95, see **Figure 16**) is higher than the one of quantile regression between 2022-02-14 and 2022-07-06 (0.74) whereas it is similar to the one of the 1st attempt with quantile regression between 2022-02-14 and 2022-02-28 (0.97). With the quantile regression of first attempt, the calibration period is much shorter where the variation in the air temperature and sensor drift have negligible effects on the sensors response, thus, the R^2 of calibration was high. **Table 7** shows that R^2 and RMSE of predicted data by multiple linear model improved respectively from 0.58 to 0.84 and from 25 ppm to 14 ppm compared to the ones by the quantile regression of the second attempt. **Figure 17** shows that a clear drift in the predicted data by the multiple linear model starting early July with a lower extendand then linearly increasing up to 40 ppm on 14 October. Finally, **Figure 18** shows that the association

of the residuals and water vapour (and relative humidity) decreases significantly, from 0.787 to 0.222, with the multiple linear regression model. However, when only the calibration period between 2022-02-14 and 2022-07-06 is examined, **Figure 19** shows that the association of water vapour (and relative humidity) and residuals disappears during the calibration period while atmospheric pressure in the measuring chamber is weakly correlated with the residuals (R^2 = 0.317).

Figure 16. SenseAir K96 sensor, calibration using multiple linear regression between 2022-02-14 and 2022-07-06 with water vapour in the measuring chamber as covariate. Up: scatterplot of calibration in minute resolution; down: time series of minute data (predicted sensor in blue and reference in red lines).

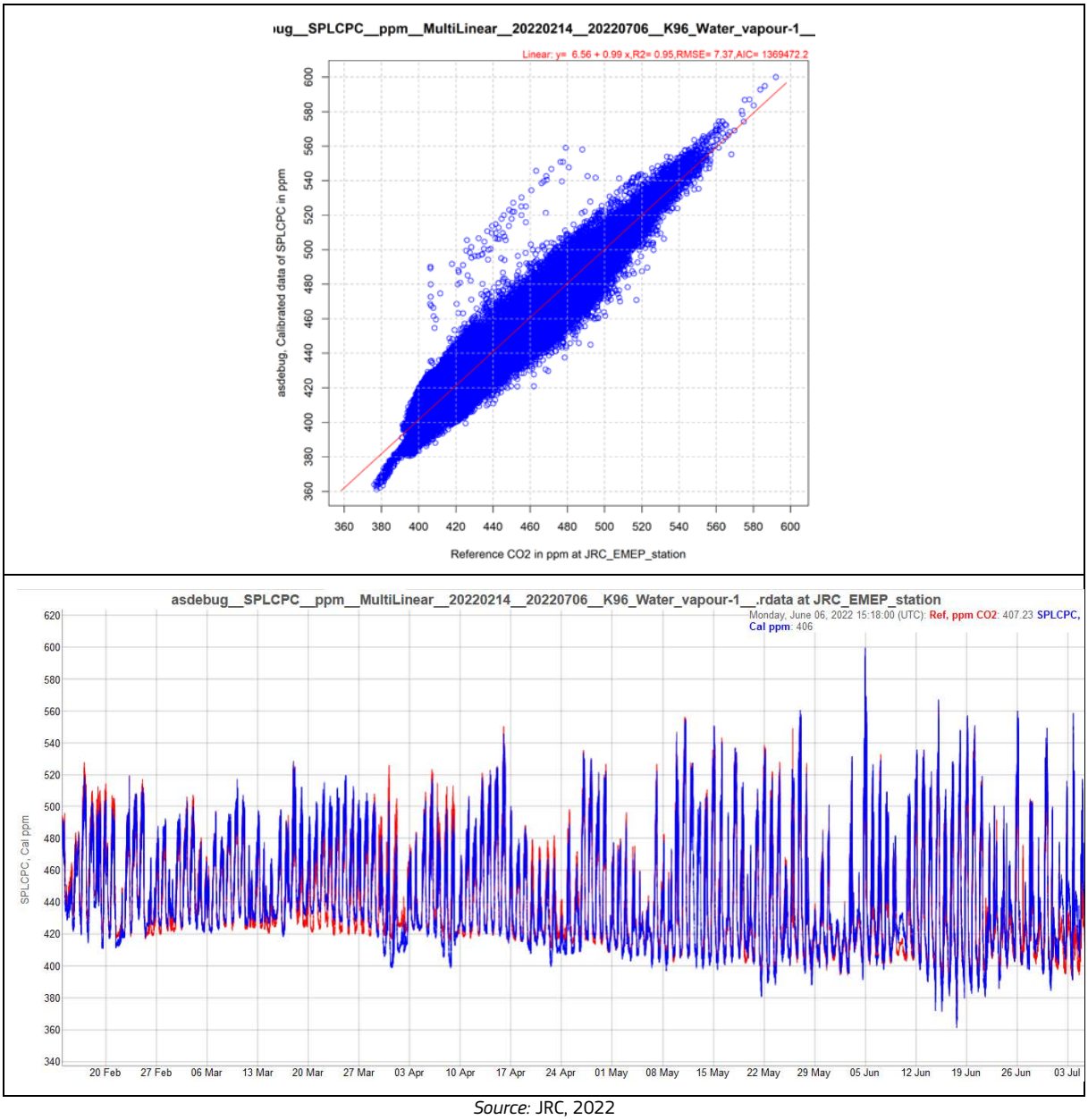

Source: JRC, 2022

Figure 17. Up: time series of hourly sensor data predicted using the multiple linear calibration model (in blue) and reference (in red); lower: daily residuals (drift). The prediction period is between 2021-12-21 and 2022-10-14.

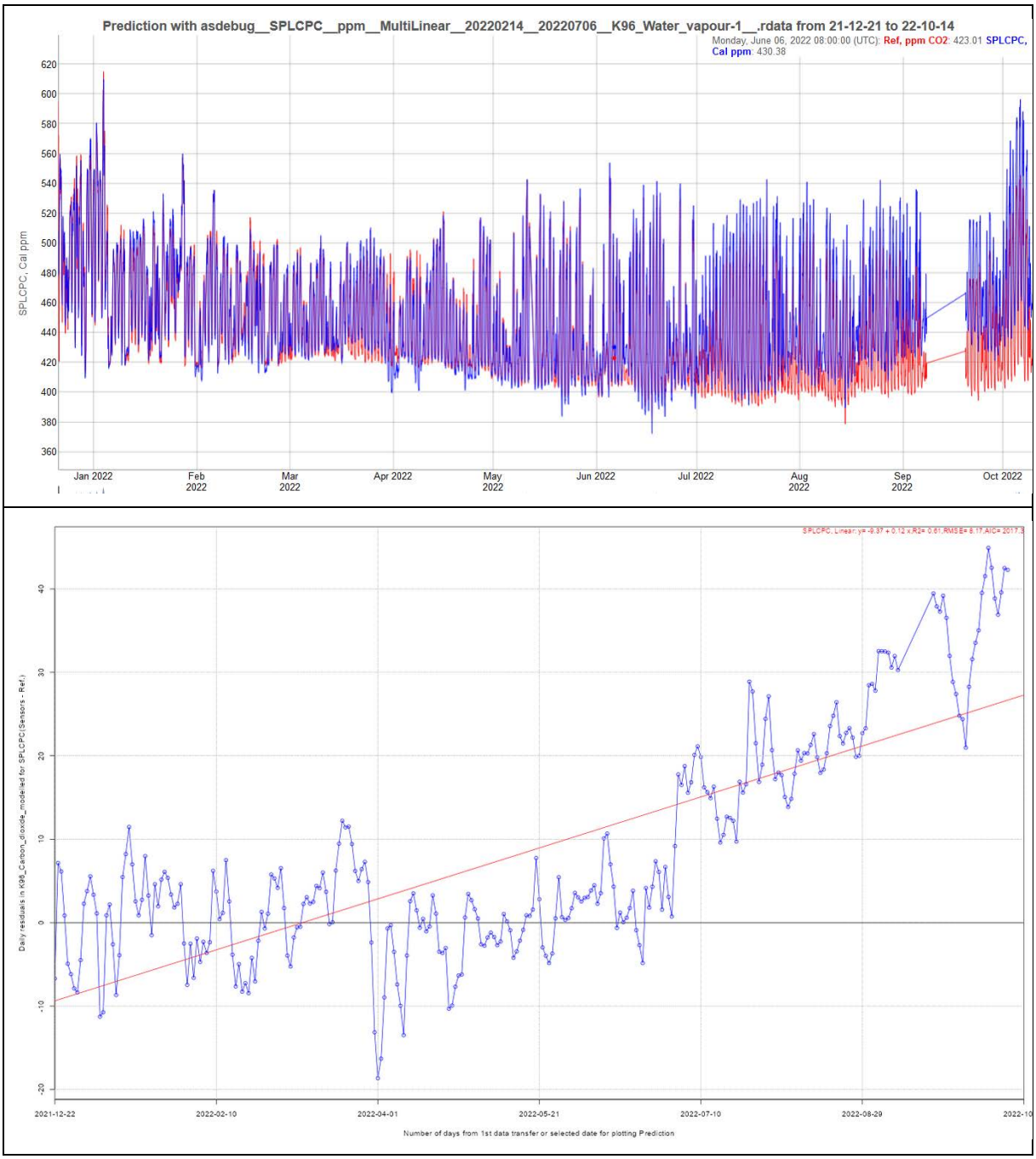

Source: JRC, 2022

Figure 18. SenseAir K96 sensor, calibrated using multiple linear model between 2022-02-14 and 2022-07-06. Plot of correlation matrix with residuals of hourly predicted data versus water vapour, atmospheric pressure, relative humidity and temperature in the SenseAir K96 measuring chamber (K96 Water vapour, K96 Atmospheric pressure, K96 Relative humidity and K96 Temperature), the Picarro CO_2 data (Ref) and the predicted CO_2 sensor data (SPLCPC Cal). The data period is between 2021-12-21 and 2022-10-14.

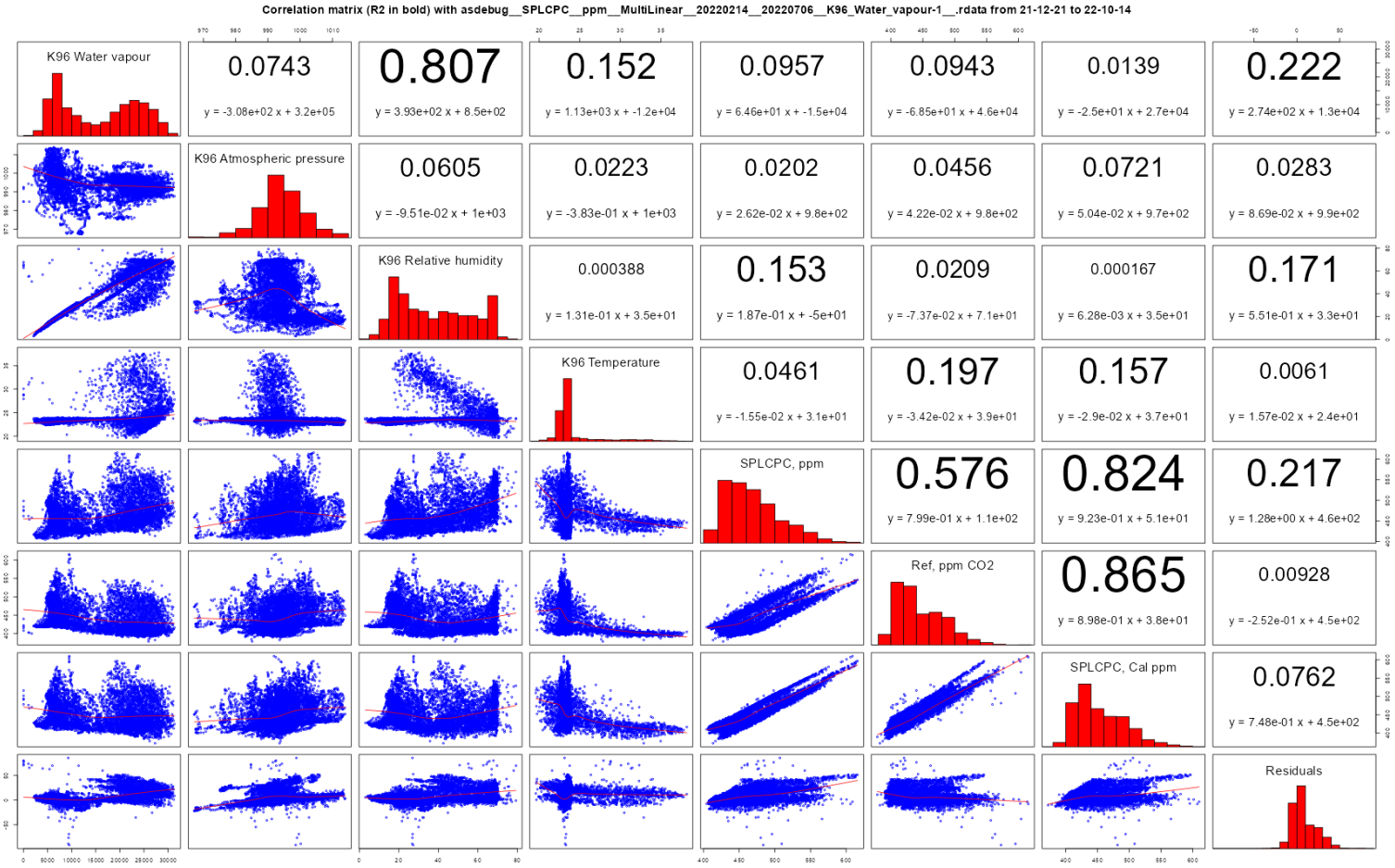

Source: JRC, 2022

Figure 19. SenseAir K96 sensor, calibrated using multiple linear model between 2022-02-14 and 2022-07-06. Plot of correlation matrix with residuals of minute predicted data versus water vapour, atmospheric pressure, relative humidity and temperature in the SenseAir K96 measuring chamber (K96 Water vapour, K96 Atmospheric pressure, K96 Relative humidity and K96 Temperature), the raw wet CO_2 sensor data (SPLCPC), the Picarro CO_2 data (Ref) and the predicted CO_2 sensor data (SPLCPC Cal). The data period is between 2022-02-14 and 2022-07—06.

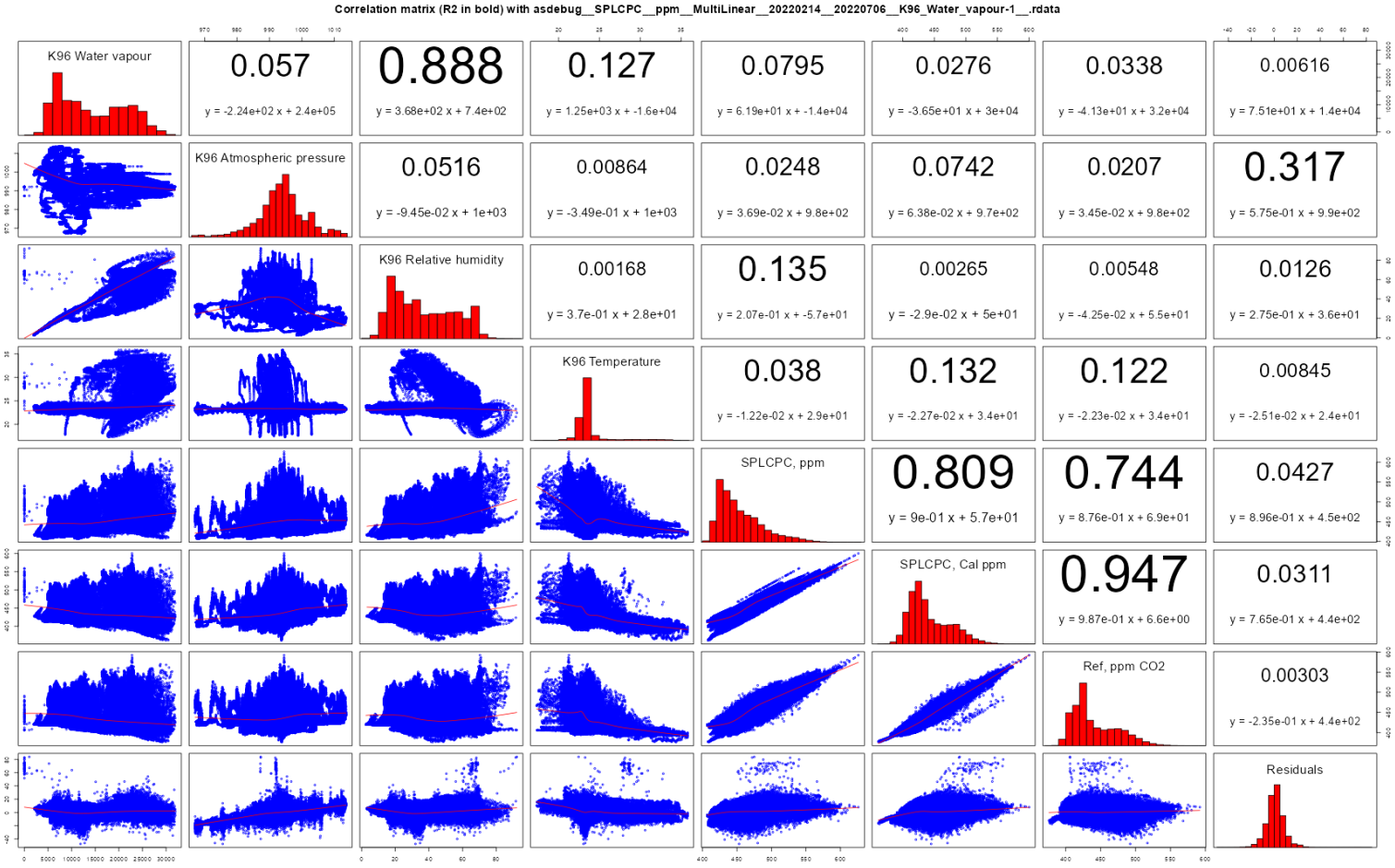

Source: JRC, 2022

Therefore, a new multiple linear model with two covariates: K96 water vapour and atmospheric pressure in the measuring chamber of the sensor was established. The calibration and prediction results of that multiple linear model are given in **Table 7**. All coefficients of the calibration model were found significantly different from 0. The R^2 of the calibration model slightly increased (0.97 compared to 0.95, see **Figure 20**). The slope, intercept, R^2 and RMSE of predicted sensor data versus reference slightly improved as well (see **Table 7**). However, **Figure 21** shows that the drift starting early July is still present with a slightly lower extent (less than 40 ppm on 14 October) compared to the multiple linear regression model using the sole water vapour (drift of 45 ppm on 14 October). The plot of residual matrix in **Figure 23** during the calibration period shows no association of any parameter with the residuals, thus adding other covariates to the calibration model is unnecessary. Nevertheless, **Figure 22** shows that for the entire series, the association of residuals and water vapour is still present. Since the drift is not observed during the calibration period, it can only be caused by the improper temperature adjustment in the measuring chamber occurring after 2022-07-06.

Figure 20. SenseAir K96 sensor, calibration using multiple linear regression between 2022-02-14 and 2022-07-06 with water vapour and atmospheric pressure in the measuring chamber as covariates. Up: scatterplot of calibration in minute resolution; down: time series of minute data (predicted sensor in blue and reference in red lines).

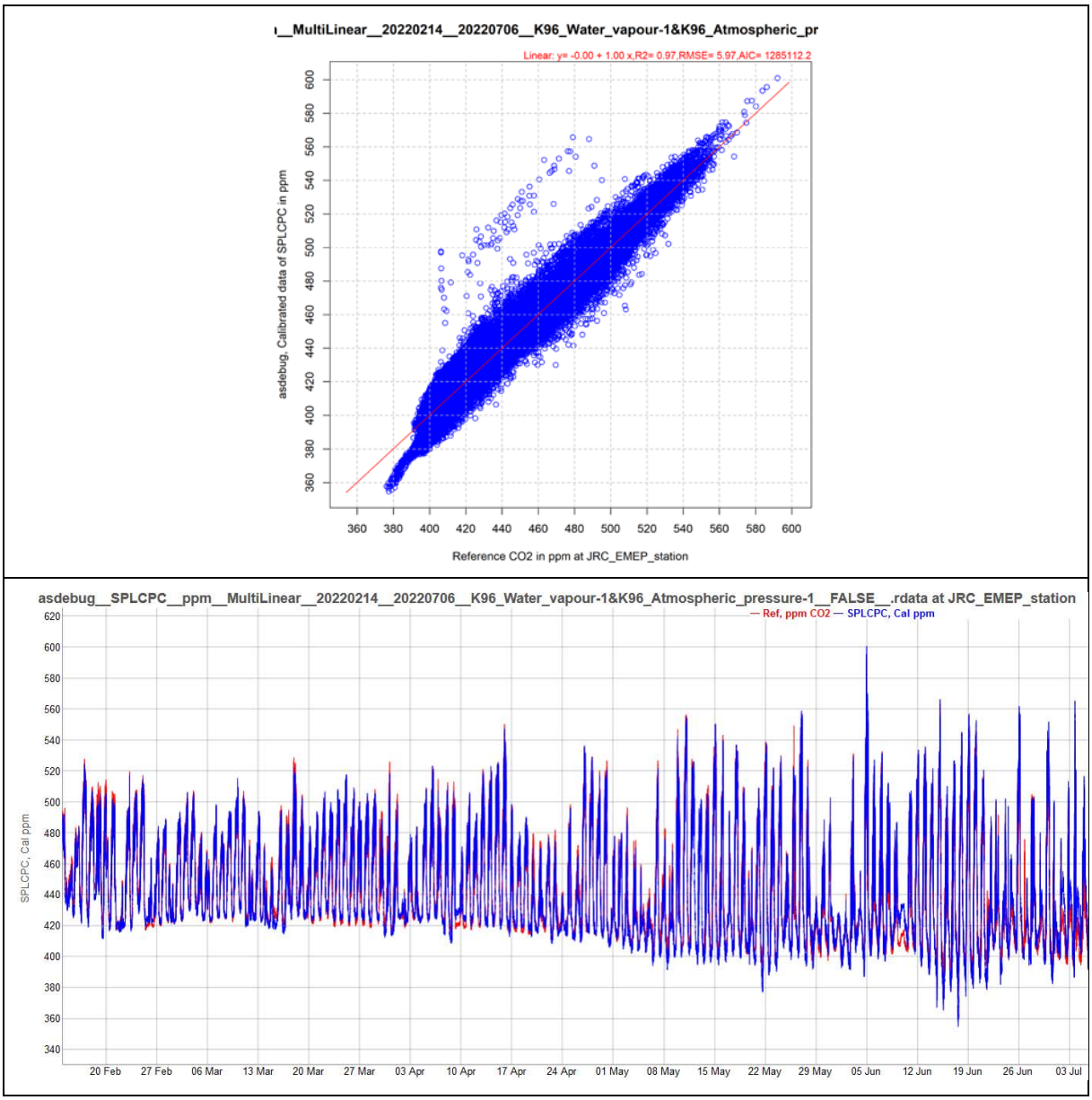

Source: JRC, 2022

Figure 21. Up: time series of hourly sensor data predicted using the multiple linear calibration model (in blue) and reference (in red); lower: daily residuals (drift). The prediction period is between 2021-12-21 and 2022-10-14.

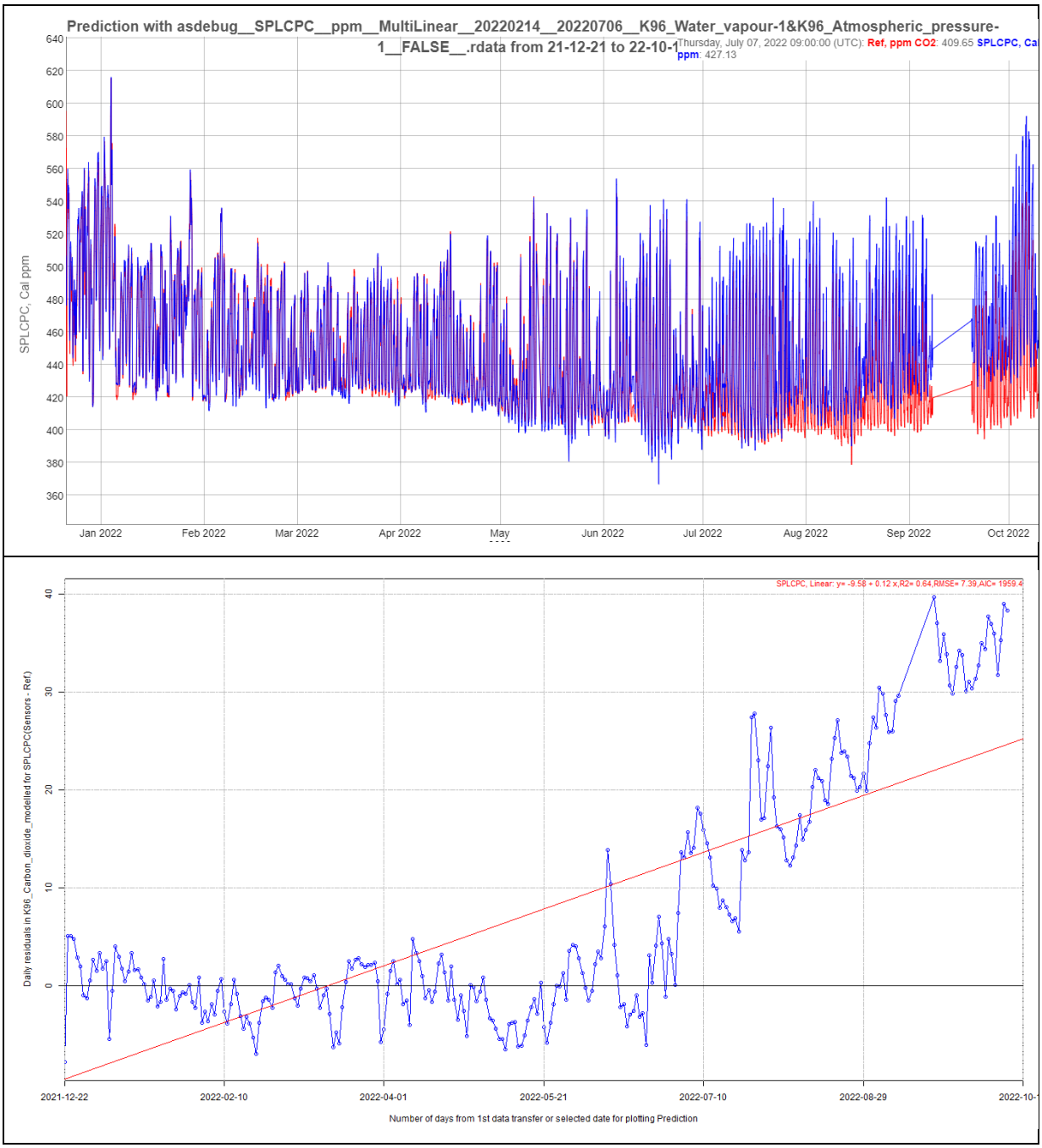

Source: JRC, 2022

Figure 22. SenseAir K96 sensor, calibrated using multiple linear model between 2022-02-14 and 2022-07-06. Plot of correlation matrix with hourly residuals of predicted data versus water vapour, atmospheric pressure, relative humidity and temperature in the SenseAir K96 measuring chamber (K96 Water vapour, K96 Atmospheric pressure, K96 Relative humidity and K96 Temperature), the raw wet CO_2 sensor data (SPLCPC), the Picarro CO_2 data (Ref) and the predicted CO_2 sensor data (SPLCPC Cal). The data period is between 2021-12-21 and 2022-10-14.

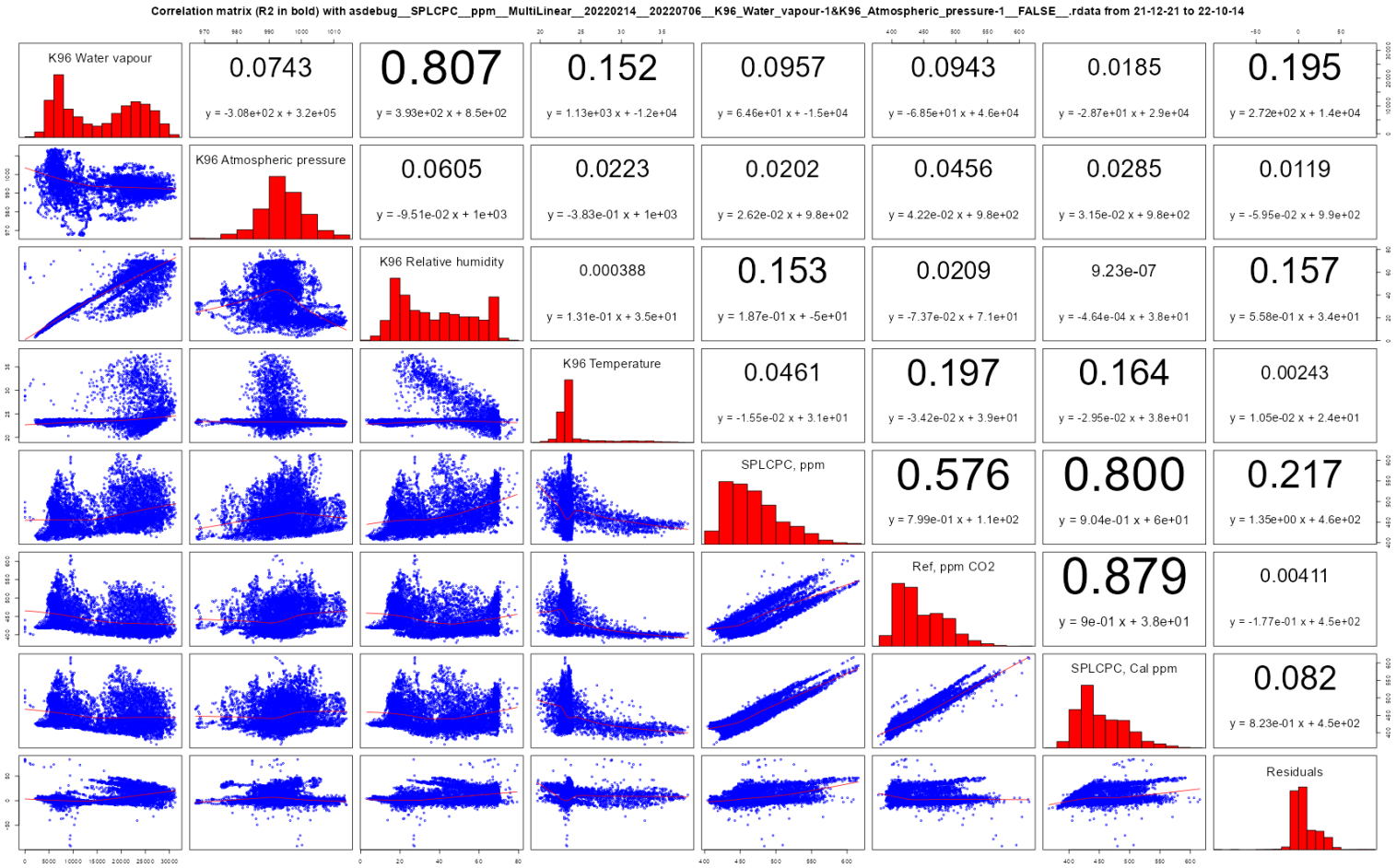

Source: JRC, 2022

Figure 23. SenseAir K96 sensor, calibrated using multiple linear model between 2022-02-14 and 2022-07-06. Plot of correlation matrix of calibration with residuals of minute predicted data versus water vapour, atmospheric pressure and temperature in the SenseAir K96 measuring chamber (K96 Water vapour, K96 Atmospheric pressure, K96 Relative humidity and K96 Temperature), the raw wet CO_2 sensor data (SPLCPC), the Picarro CO_2 data (Ref) and the predicted CO_2 sensor data (SPLCPC Cal).

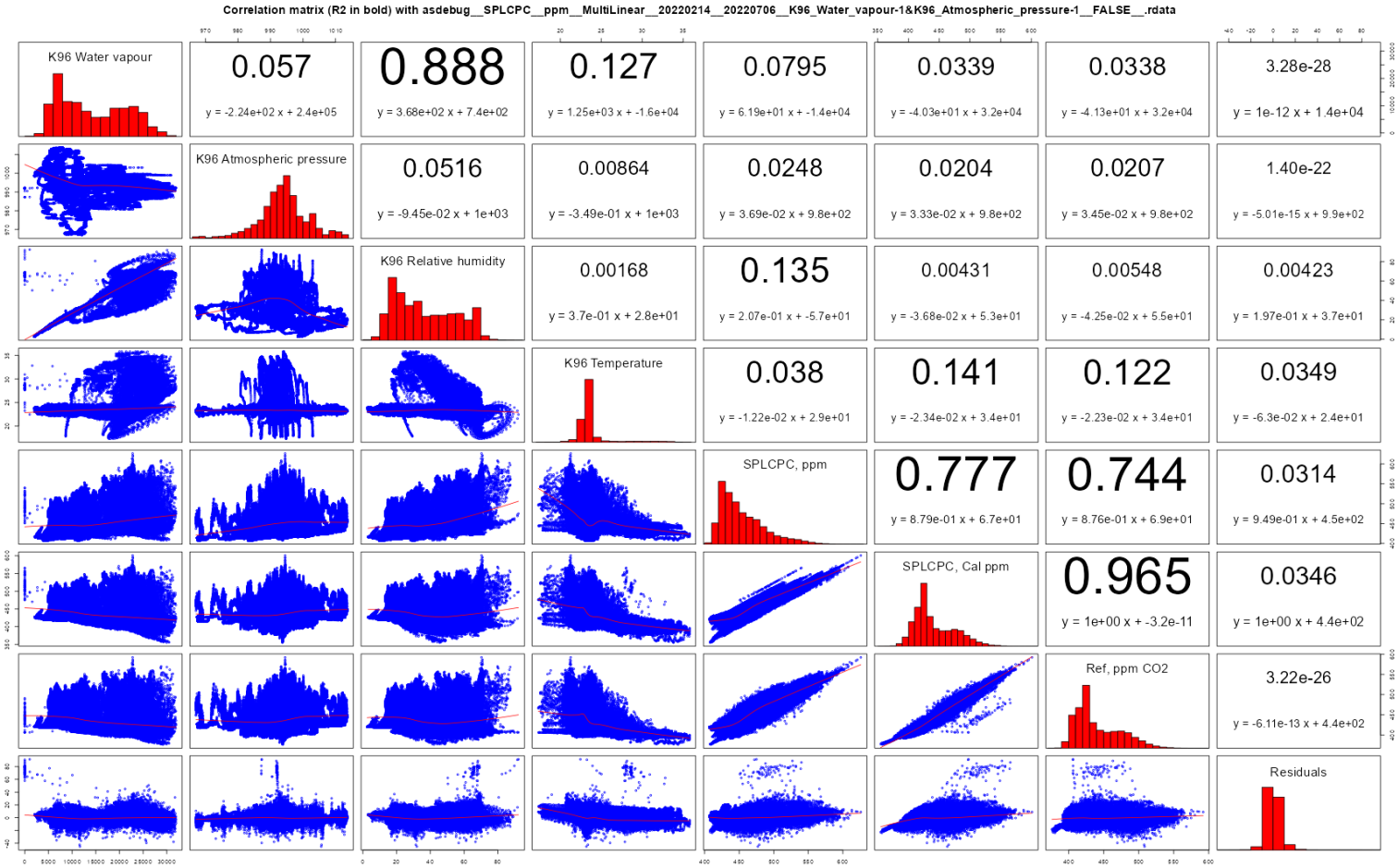

Source: JRC, 2022

Figure 24 gives the scatterplot of the entire time series of hourly predicted CO_2 sensor versus CO_2 Picarro reference data with the sensor being calibrated between 20-02-14 and 2022-07-06 using the multiple linear model with water vapour and pressure as covariates. The scatterplot clearly shows two populations of sensor data that correspond to the change in temperature control regime in the measuring chamber. One population ends up around early July showing a slope about 1 and intercept about 0. The second one starts early July with higher air temperature and it has a similar slope and an increased intercept up to 40 ppm.

Figure 24. Scatterplot of the hourly predicted CO_2 sensor data calibrated with multiple linear model and water vapour and pressure as covariate between 20-02-14 and 2022-07-06 versus CO_2 Picarro reference data

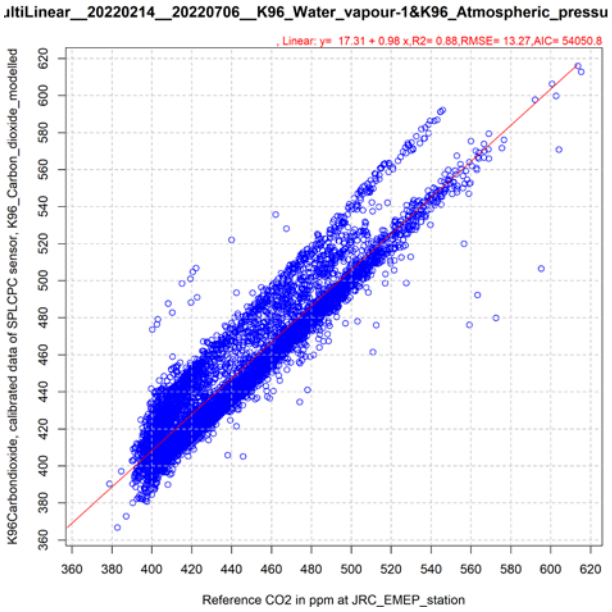

Source: JRC, 2022

4.3 The effectiveness of temperature controlled chamber

The target temperature for measuring chamber containing the CO_2 sensor was 25 °C over the whole field experiment. The temperature control system was effective until mid-June 2022 when the summer temperature starts increasing strongly. From that date until mid-September, the AirSensEUR sensor system used 100% of available energy for cooling down in order to maintain 25 °C in the measuring chamber but without success, see **Figure 25**. K96_Temperature and K96_Chamber_Temperature started increasing with a few peaks in May and constantly from June 2022 until early September 2022. The temperature control system was again effective from mid-September onward.

Figure 25. Efficiency of temperature controlled system in the AirSensEUR unit. K96_Temperature is the temperature in the sensor, K96_Chamber_Temperature is the CO_2 Internal chamber temperature at the center of the board, Temperature is the ambient air temperature outside AirSensEUR, Temperature_int is the temperature of the electronic of AirSensEUR

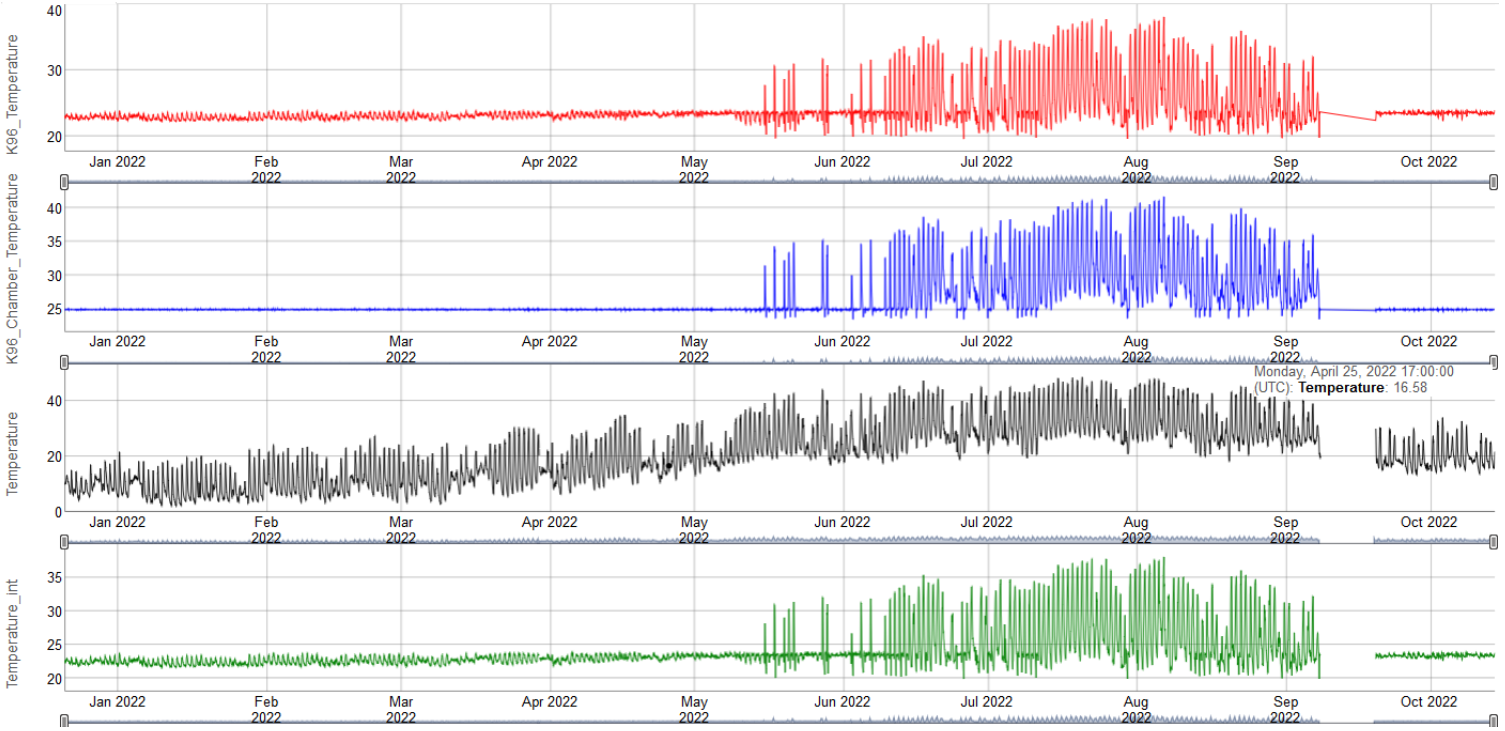

Source: JRC, 2022

Due to inefficient temperature control, we tried using temperature in the K96 sensor rather than water vapour as the first covariate of a new multiple linear model. Similar to the calibration with the sole water vapour, the residuals of the calibration model using the sole temperature showed a mild correlation with atmospheric pressure and a huge one with water vapour.

Therefore, we fitted a last multiple linear model with three covariates: temperature and atmospheric pressure in the measuring chamber of the sensor together with water vapour measured by the K96 sensor. The calibration period was between 2022-04-01 and 2022-06-01, which was selected to cover the time with high air temperature . The calibration and prediction results of the last multiple linear model are given in **Table 7**. All coefficients of the calibration model were found significantly different from 0. The R^2 of the calibration model slightly improved compared to the ones of preceding model (0.99 instead of 0.97, see **Figure 26**). Conversely, the slope, intercept, R^2 and RMSE of hourly predicted sensor data versus reference data of the whole data series slightly worsened compared to the ones of calibration model with water vapour and atmospheric pressure (see **Table 7**). **Figure 27** also shows a slight worsening in the drift ending over 40 ppm on 14 October. The plot of residual matrix (**Figure 29**) of calibration period shows no association between residuals and any parameter, thus adding other covariates to the calibration model is unnecessary. Nevertheless, **Figure 28** shows that for the entire data series, the association between the residuals and water vapour considerably worsened compared to the one by multiple linear model with water vapour and atmospheric pressure as covariates (see **Figure 22**), which remains the best calibration model.

Figure 26. SenseAir K96 sensor, calibration using multiple linear regression between 2022-04-01 and 2022-06-01 with temperature and atmospheric pressure in the measuring chamber as covariates. Up: scatterplot of calibration in minute resolution; down: time series of minute data (predicted sensor in blue and reference in red lines).

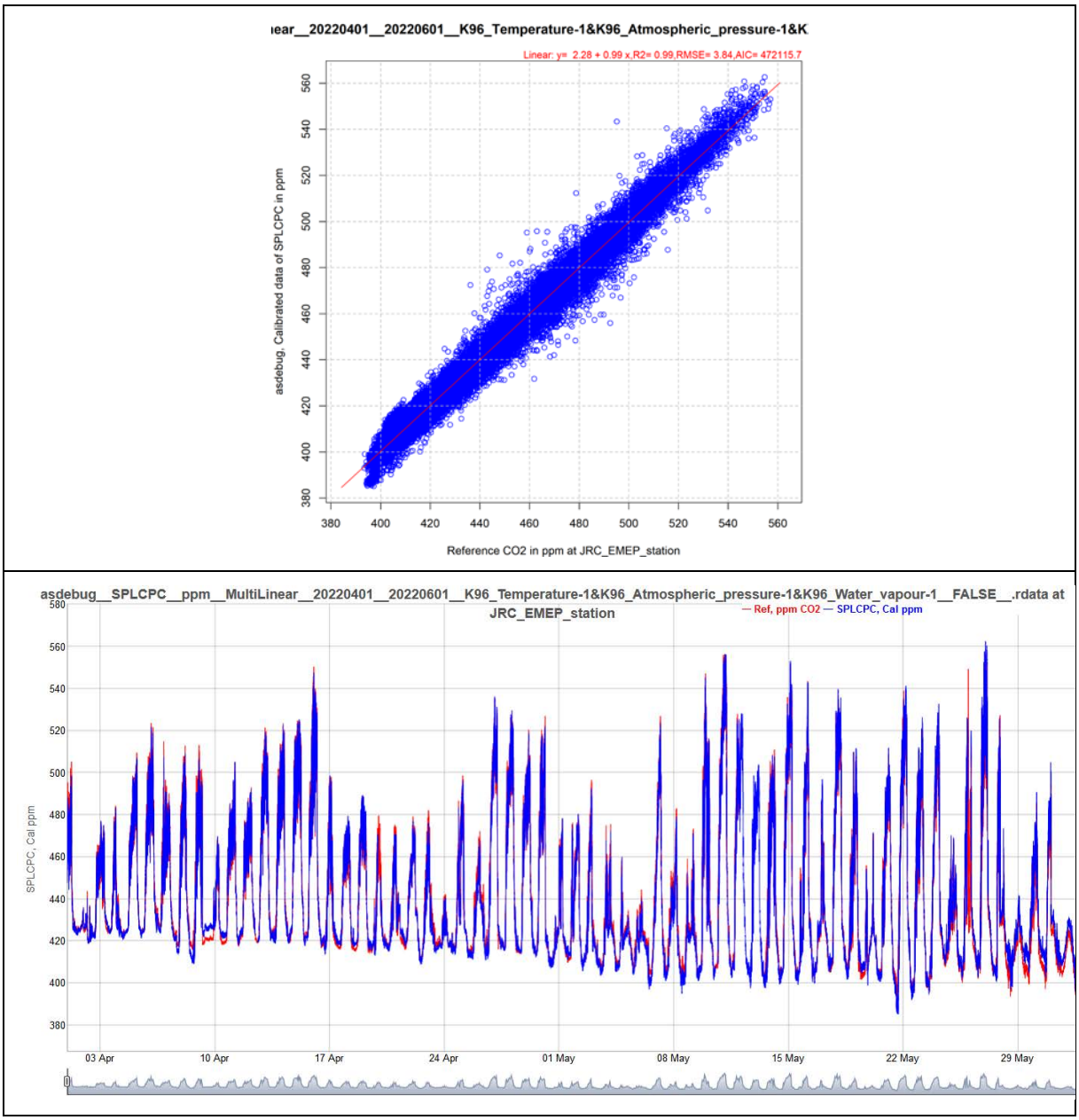

Source: JRC, 2022

Figure 27. Up: time series of hourly sensor data predicted using the multiple linear calibration model (in blue) and reference (in red); down: daily residuals (drift). The prediction period is between 2021-12-21 and 2022-10-14.

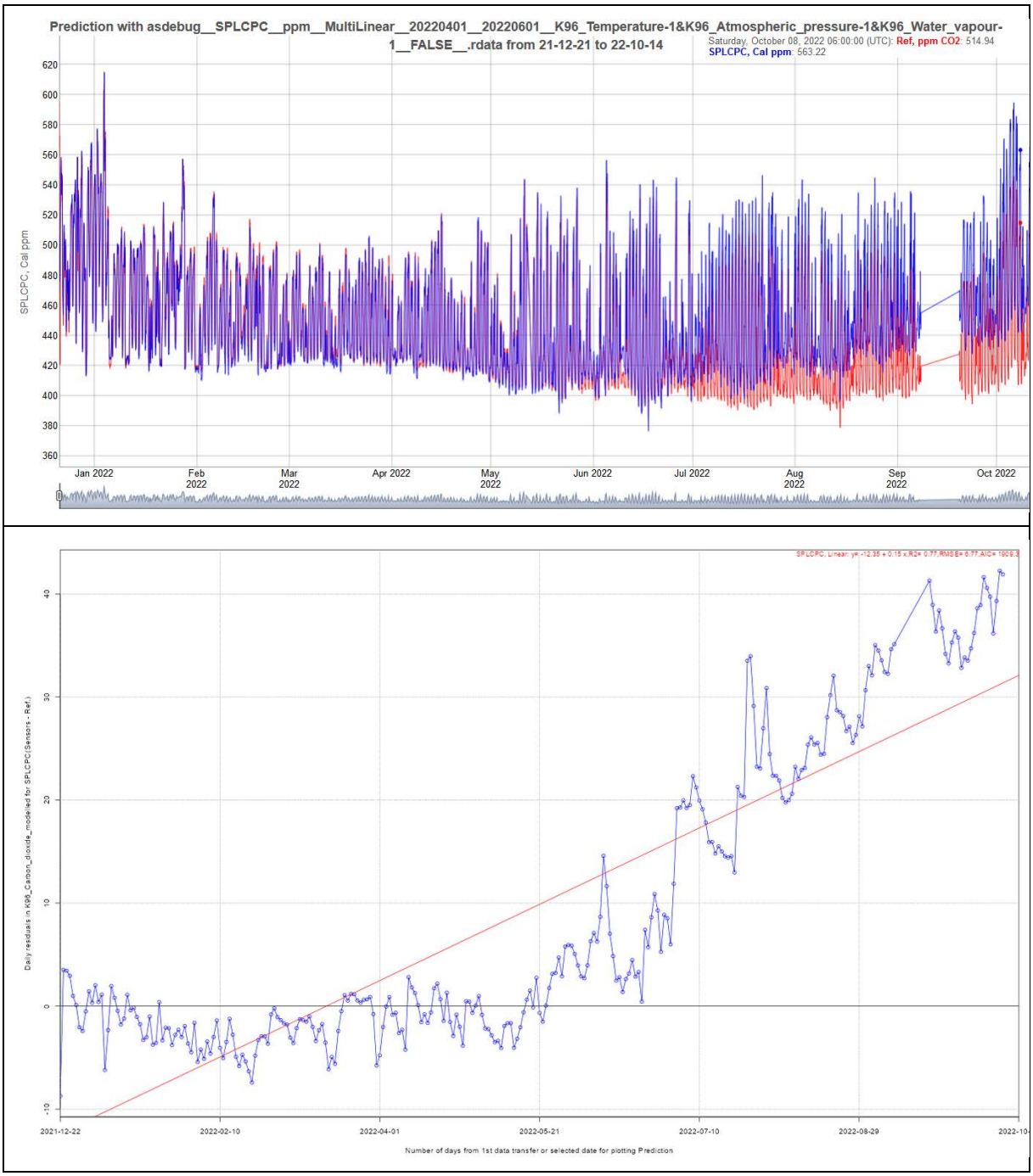

Source: JRC, 2022

Figure 28. SenseAir K96 sensor, calibrated using multiple regression model between 2022-04-01 and 2022-06-01. Plot of correlation matrix with hourly residuals of predicted data versus water vapour, atmospheric pressure and temperature in the SenseAir K96 measuring chamber (K96 Water vapour, K96 Atmospheric pressure, K96 Relative humidity and K96 Temperature), the Picarro CO_2 data (Ref) and the predicted CO_2 sensor data (SPLCPC Cal). The data period is between 2021-12-21 and 2022-10-14.

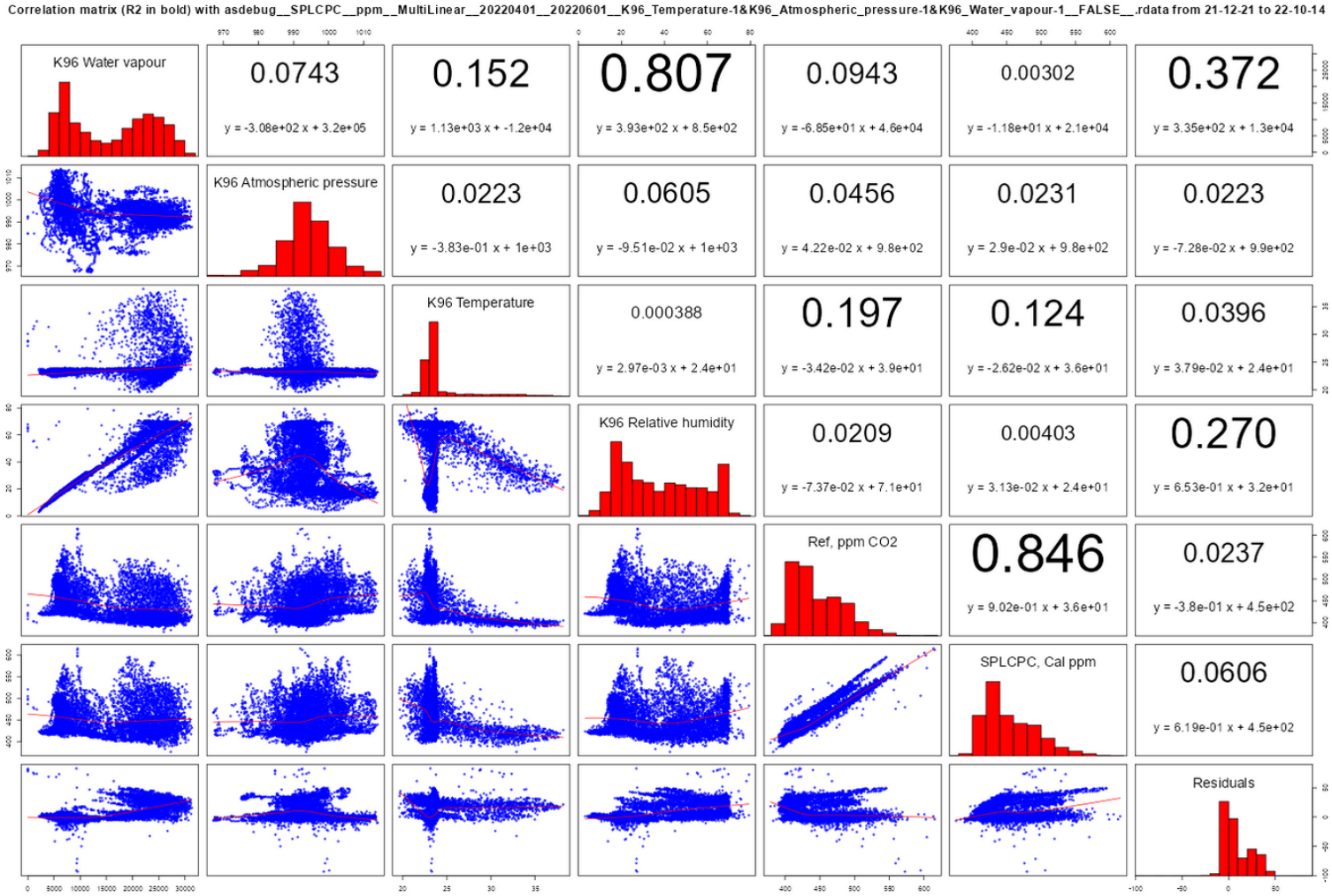

Source: JRC, 2022

Figure 29. SenseAir K96 sensor, calibrated using multiple linear model between 2022-04-01 and 2022-06-01. Plot of correlation matrix in the calibration with residuals of minute predicted data versus water vapour, atmospheric pressure and temperature in the SenseAir K96 measuring chamber (K96 Water vapour, K96 Atmospheric pressure, K96 Relative humidity and K96 Temperature), the Picarro CO_2 data (Ref) and the predicted CO_2 sensor data (SPLCPC Cal).

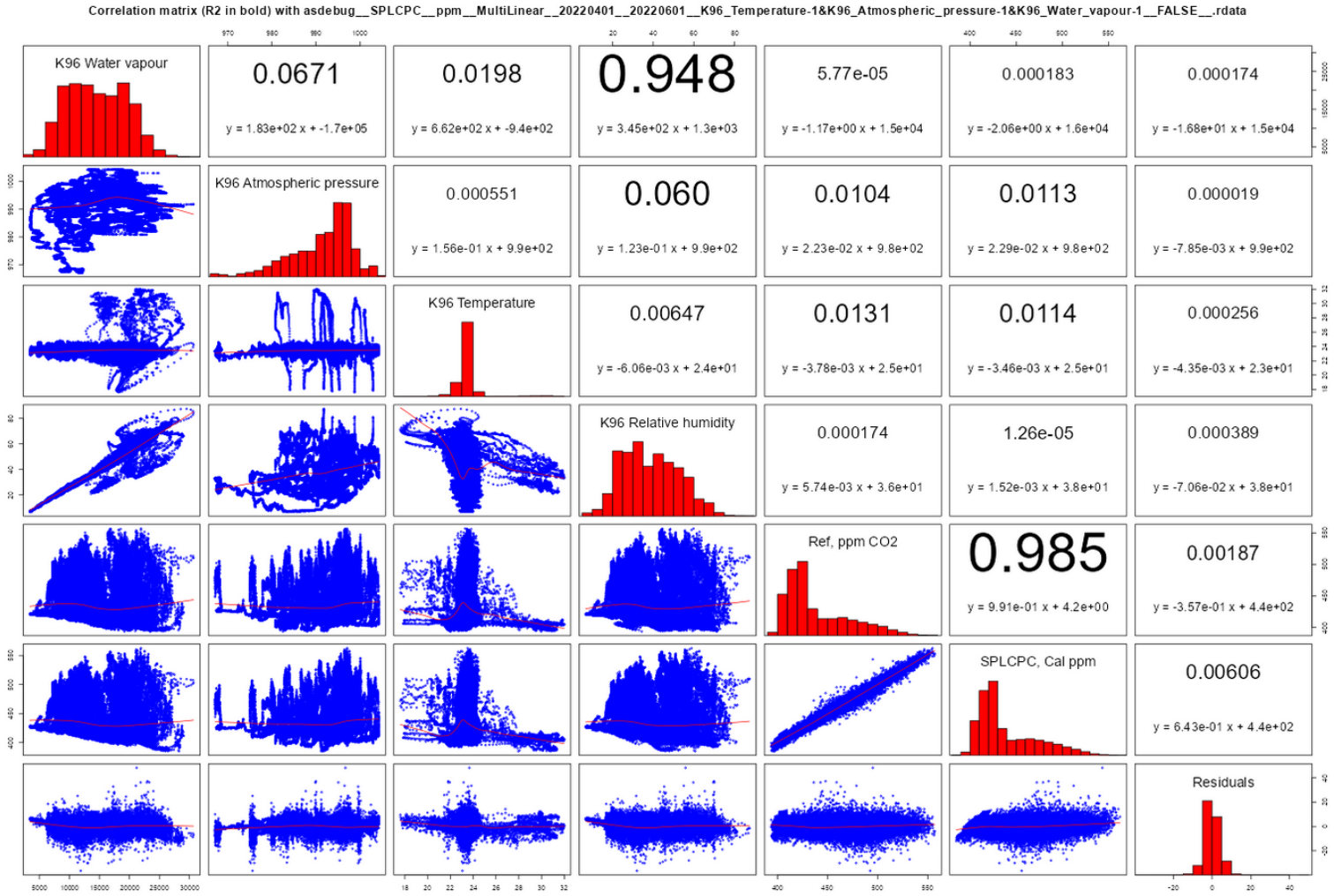

Source: JRC, 2022

5 Meeting Data Quality objective and drift over time of CO_2 sensor

Figure 24 shows that there is a linear relationship between the predicted CO_2 sensor data (Y) and the CO_2 Picarro reference data (X) that can be described by Equation 3.

$$Y = b_0 + b_1 X \qquad \text{Equation 3}$$

where

Y is the hourly CO_2 predicted data series;

X is hourly CO_2 Picarro reference data series, which is the best estimation of true values;

b_0 and b_1 are respectively the intercept and slope of the regression line of Y against X.

Table 7 includes the b_1 (as slope), b_0 (as intercept) and RMSE of Ordinary Least Square regression line. In addition, for the quantitative assessment, the expanded uncertainty of predicted CO_2 sensor data, U(Y), was estimated using Equation 4 to check if the DQOs defined in section 1 is met:

$$U(Y) = k\left(\frac{\mathrm{RSS}}{N-2} - u^2(bs,RM) + [b_0 + (b_1 - 1)\mathrm{X}]^2\right)^{½} \qquad \text{Equation 4}$$

Where:

- k is the coverage factor accounting for the probability distribution of uncertainty of a measurement with a selected probability level. The corresponding standard (CEN, 2021) imposes k to be 2 for a large number of experimental results available that gives approximately the 95% confidence interval for a normal distribution (1.96 at 95% confidence level),
- u(bs,RM) is the between reference method standard uncertainty set to 0.1 ppm for the Picarro G2401,
- N is the number of data pairs,
- RSS is the sum of the squared residuals, computed using Equation 5, when the RSS is constant over the X range:

$$\mathrm{RSS} = \sum [Y - (b_0 + b_1 X)]^2 \qquad \text{Equation 5}$$

The RSS includes the random uncertainty of reference measurements. u(bs,RM) shall be subtracted from the RSS, thanks to $(\mathrm{RSS}/(n-2))^{1/2}$ and u(bs,RM) being independent and therefore their variances are additive.

In Equation 5, the residuals, , $(\mathrm{Y} - (b_1 X + b_0))$, are assumed to be fairly constant over X range to attribute an X-regardless value to the RSS. Equation 5 is valid only if the variance of residuals remains constant over X range, so-called homogeneity of variance or homoscedasticity. Conversely, the situation of the variance of residuals varying over X is called heterogeneity of variance or heteroscedasticity (Zuur et al., 2010). Heteroscedasticity was detected in our dataset using the Breusch Pagan test (Breusch and Pagan, 1979). Therefore, using the RSS in Equation 5 was not possible since the squares of residuals, RS_i, are not constant over X range. However, a simple approach to account for possible heteroscedasticity consisted of fitting a General Additive Model (GAM) (Hastie and Tibshirani, 1990) describing the relationship between relative residual (RS) and X, and thus the modifications of Equation 4 to Equation 6 for computing U(Y).

$$U(Y) = k(\mathrm{RS} - u^2(bs,RM) + [b_0 + (b_1 - 1)\mathrm{X}]^2)^{½} \qquad \text{Equation 6}$$

In section 1, we defined a DQO expressed as expanded uncertainty of measurements for CO_2 sensor of 10 ppm. **Figure 30** shows the expanded uncertainty of CO_2 sensor measurement calibrated with multiple linear model with water vapour and pressure as covariates between 20-02-14 and 2022-07-06. The upper of **Figure 30** gives the expanded uncertainty of CO_2 sensor measurements for the entire time series between 2021-12-21 and 2022-10-14. It shows that for the CO_2 range between 380 and 550 ppm, the expanded uncertainty ranged between 20 and 25 ppm. The sharp increase in the expanded measurement uncertainty at CO_2 concentrations over 550 ppm is caused by the small number of data points (see **Figure 24**) resulting in high RS value when fitting a GAM model. The major contribution to the expanded uncertainty comes from the bias given in Equation 6: $b_0 + (b_1 - 1)X$. This resulted from the drift of the sensor starting in early July 2022 likely caused by the increased of temperature in the measurement chamber.

In fact, when limiting the time series to the period when the temperature in the measuring chamber was well-controlled to 25 °C, the expanded uncertainty of measurement remained below 10 ppm for the CO_2 range between 400 to 550 ppm.

Figure 30. Expanded uncertainty of predicted CO_2 sensor data calibrated using multiple linear model with water vapour and pressure as covariates between 20-02-14 and 2022-07-06. Up: the entire time series from 2021-12-21 to 2022-10-14 ; down: the time series from 2021-12-21 to 2022-07-06 when the temperature control system could maintain the temperature in measuring chamber at 25°C

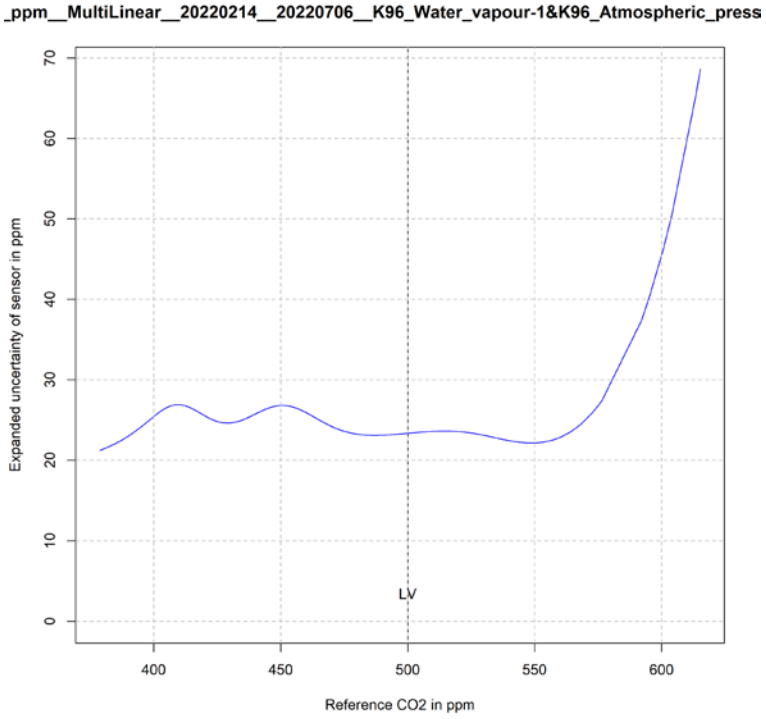

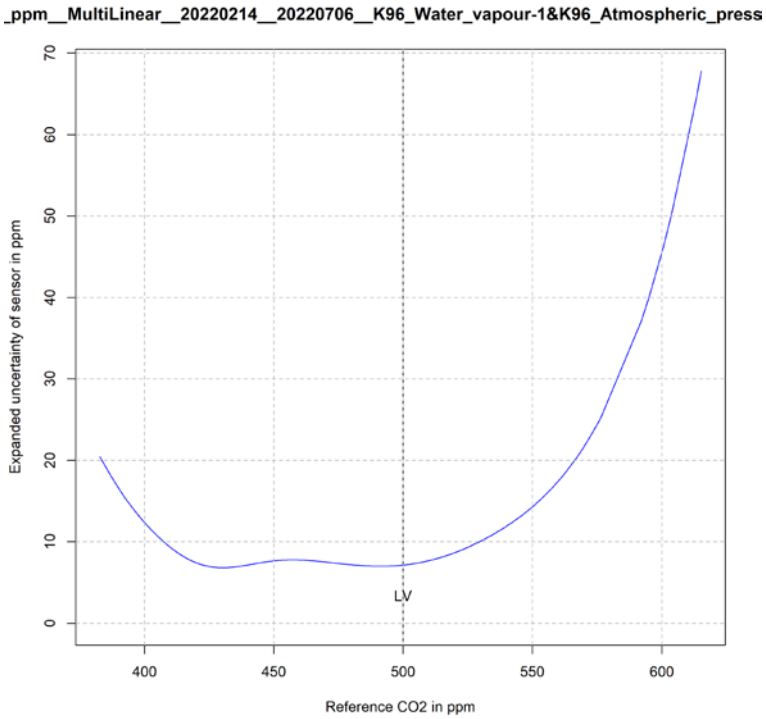

Source: JRC, 2022

6 Conclusion

We have tested the K96 Senseair CO_2 LCS at the JRC observatory station since December 2021 in order to evaluate whether the expanded uncertainty of sensor measurement can meet a data quality objective of 10 ppm.

We calibrated the wet CO_2 LCS data against the wet CO_2 Picarro reference measurements. The linear models were found inadequate since their residuals were strongly associated with water vapour and temperature in the measuring chamber and with air pressure at a lower extent. A multiple linear regression model using water vapour and air pressure in the measuring chamber as covariates was finally used for calibration. Since water vapour and temperature were strongly correlated, it was not feasible to add them both in the calibration model.

Applying this calibration model for prediction, the expanded uncertainty of measurements was found ranging between 20 and 25 ppm when CO_2 ranged from 380 to 550 ppm, which exceeded the DQO of 10 ppm.

However, the LCS showed a strong drift in summer when the target temperature in the measuring chamber could not be maintained during the high temperature episodes, even though full capacity of the energy available for chamber cooling was used. In fact, the expanded uncertainty of sensor measurement reduced to 10 ppm for the time series between 2021-12-21 and 2022-07-06, when the temperature of chamber was well-maintained.

The temperature in the measuring chamber returned to the target value of 25 °C from mid-September 2022. However, while the chamber temperature was stable at the target value onwards, the residuals of LCS measurements did not return to zero and remained around 35 ppm. It seems that the high temperature led to a permanent effect on the LCS. One may assume a change in the optical path, laser and detector positioning due to the dilation inside the sensor that is irreversible.

Nevertheless, the results obtained so far are promising, as the DQO is met until temperature in the measuring chamber started increasing, and further experiments should be carried out after addressing the following suggestions:

- Improve the insulation of temperature controlled chamber and the efficiency of its PID control system on temperature;
- Protect the AirSensEUR from direct sunlight by mounting it into a weather instrument shelter;
- Change the target temperature of measuring chamber to be over 25 °C in order to maintain the efficient cooling during high summer air temperatures.

References

2008/50/EC: Directive of the European Parliament and of the Council of 21 May 2008 on ambient air quality and cleaner air for Europe [WWW Document], n.d. URL https://eur-lex.europa.eu/eli/dir/2008/50/oj (accessed 8.22.19).

Breusch, T., Pagan, A., 1979. A Simple Test for Heteroscedasticity and Random Coefficient Variation. Econometrica 47, 1287–94.

CEN/TS 17660-1 Air quality — Performance evaluation of air quality sensor systems — Part 1: Gaseous pollutants in ambient air [WWW Document], 2021. URL https://www.boutique.afnor.org/en-gb/standard/din-cen-ts-176601/air-quality-performance-evaluation-of-air-quality-sensor-systems-part-1-gas/eu174644/322334 (accessed 10.7.21).

Draper, N.R., Smith, H., 1998. Applied Regression Analysis, 3rd Edition | Wiley.

Harmon, T.C., Dierick, D., Trahan, N., Allen, M.F., Rundel, P.W., Oberbauer, S.F., Schwendenmann, L., Zelikova, T.J., 2015. Low-cost soil CO2 efflux and point concentration sensing systems for terrestrial ecology applications. Methods in Ecology and Evolution 6, 1358–1362. https://doi.org/10.1111/2041-210X.12426

Hastie, T.J., Tibshirani, R.J., 1990. Generalized Additive Models, New York: Chapman and Hall.

Koenker, R., code), S.P. (Contributions to C.Q., code), P.T.N. (Contributions to S.Q., code), A.Z. (Contributions to dynrq code essentially identical to his dynlm, code), P.G. (Contributions to nlrq, advice), B.D.R. (Initial (2001) R. port from S. (to my everlasting shame--how could I. have been so slow to adopt R. and for numerous other suggestions and useful, 2018. quantreg: Quantile Regression.

Wastine, B., Hummelgård, C., Bryzgalov, M., Rödjegård, H., Martin, H., Schröder, S., 2022. Compact Non-Dispersive Infrared Multi-Gas Sensing Platform for Large Scale Deployment with Sub-ppm Resolution. Atmosphere 13, 1789. https://doi.org/10.3390/atmos13111789

Yasuda, T., Yonemura, S., Tani, A., 2012. Comparison of the Characteristics of Small Commercial NDIR CO2 Sensor Models and Development of a Portable CO2 Measurement Device. Sensors 12, 3641–3655. https://doi.org/10.3390/s120303641

Yatkin, S., Gerboles, M., Borowiak, A., Signorini, M., 2022. Guidance on low-cost sensors deployment for air quality monitoring experts based on the AirSensEUR experience [WWW Document]. JRC Publications Repository. https://doi.org/10.2760/14893

Zuur, A.F., Ieno, E.N., Elphick, C.S., 2010. A protocol for data exploration to avoid common statistical problems. Methods in Ecology and Evolution 1, 3–14. https://doi.org/10.1111/j.2041-210X.2009.00001.x

List of abbreviations and definitions

ASE_App	shiny app developed at JRC for the data management and treatment of AirSensEUR sensor data.
CH_4	Methane
CO_2	Carbon dioxide
DQO	Data quality objectives
H_2O	water vapour
ICOS	Integrated Carbon Observation System
JRC	Joint Research Centre
N_2O	nitrous oxide
LCS	Low Cost Sensor
OECD	Organisation for Economic Co-operation and Development
SS_{res}	sum square of residuals

List of figures

List of tables

GETTING IN TOUCH WITH THE EU

In person

All over the European Union there are hundreds of Europe Direct centres. You can find the address of the centre nearest you online (european-union.europa.eu/contact-eu/meet-us_en).

On the phone or in writing

Europe Direct is a service that answers your questions about the European Union. You can contact this service:

— by freephone: 00 800 6 7 8 9 10 11 (certain operators may charge for these calls),

— at the following standard number: +32 22999696,

— via the following form: european-union.europa.eu/contact-eu/write-us_en.

FINDING INFORMATION ABOUT THE EU

Online

Information about the European Union in all the official languages of the EU is available on the Europa website (european-union.europa.eu).

EU publications

You can view or order EU publications at op.europa.eu/en/publications. Multiple copies of free publications can be obtained by contacting Europe Direct or your local documentation centre (european-union.europa.eu/contact-eu/meet-us_en).

EU law and related documents

For access to legal information from the EU, including all EU law since 1951 in all the official language versions, go to EUR-Lex (eur-lex.europa.eu).

Open data from the EU

The portal data.europa.eu provides access to open datasets from the EU institutions, bodies and agencies. These can be downloaded and reused for free, for both commercial and non-commercial purposes. The portal also provides access to a wealth of datasets from European countries.

The European Commission's science and knowledge service

Joint Research Centre

JRC Mission

As the science and knowledge service of the European Commission, the Joint Research Centre's mission is to support EU policies with independent evidence throughout the whole policy cycle.

EU Science Hub
joint-research-centre.ec.europa.eu

@EU_ScienceHub

EU Science Hub - Joint Research Centre

EU Science, Research and Innovation

EU Science Hub

EU Science

Publications Office
of the European Union